OCR

INFORMATION REPORT INFORMATION REPORT

CENTRAL INTELLIGENCE AGENCY

C-O-N-F-I-D-E-N-T-I-A-L

COUNTRY East Germany

SUBJECT Monthly Technical Review (technical & scientific articles on measuring instruments)

REPORT

DATE DISTR. 24 APR 1958

NO. PAGES 1

REFERENCES RD

25X1

DATE OF INFO.

PLACE & DATE ACQ.

Reel # 413

25X1

SOURCE EVALUATIONS ARE DEFINITIVE. APPRAISAL OF CONTENT IS TENTATIVE.

[redacted] a pamphlet issued by VEB Elektro-Apparate-Werke Treptow on measuring instruments, containing technical and scientific articles.

[redacted] Comment: The pamphlet is not classified when detached from the covering report. 25X1

[redacted]

25X1

URE ATTACHED
LEASE ROUTE

11 JUN 1958

C-O-N-F-I-D-E-N-T-I-A-L

STATE	X	ARMY	X	NAVY	X	AIR	X	FBI		AEC					

(Note: Washington distribution indicated by "X"; Field distribution by "#".)

INFORMATION REPORT INFORMATION REPORT

Monthly Technical Review

VOLUME 1 NUMBER 10 DECEMBER 1957 PAGES 233—240

VEB VERLAG TECHNIK BERLIN 10/1957

Amateur-film black-and-white and coloured

Agfacolor-kine-film

Kine-film black-and-white 35 and 16 mm

Roentgen- and technical films

VEB FILMFABRIK

AGFA WOLFEN

Wolfen Kr. Bitterfeld

CONTENTS

In forthcoming issues:

On the Separation of Solid Particles from Liquids by Hydro-Cyclones — *Lindner*

Zeiss Planetarium for the City of Calcutta — *Beck*

The Development of Hi h-Speed Low Weight Turbo-Compressors in the German Democratic Republic — *Christof*

Plane Cam Connecting-Rod Gears — *Mueller*

Subscription to
"Monthly Technical Review"

to be addressed to:
from the whole world to
VEB Verlag Technik,
Berlin C 2, Oranienburger Str. 13/14.

Australia: Continental Bookshop,
300 Little Collins Street, Melbourne C 1, Victoria
Current Book Distributor,
40 Market Street, Sydney

China: Guozi Shudian, Suchou Hutung 38,
Peking

Greece: Georg Mazarakis & Co.,
Patissionstr. 9, Athen

India: S. K. Bose, G. P. O. Box 2662, Calcutta–1
People's Publishing House, Ltd.
Khanna Bldgs., Opp. Irwin Hospital, New Delhi

Indonesia: Pembangunan Ltd., Postbox 33,
Djakarta

Japan: Far Eastern Book Sellers, Kanda P. O. Box 72,
Tokyo

South Africa: Universitas-Books, P. O. Box 1557,
Pretoria

Sweden: AB Henrik Lindstahls Bokhandel,
Odengatan 22, Stockholm

Switzerland: Pinkus & Co., Büchersuchdienst,
Predigergasse 7, Zürich I

Published by: VEB Verlag Technik,
Berlin C 2, Oranienburger Str. 13/14

Monthly Technical Review
Chief Editor: *Max Kühn*, Berlin W 8, Unter den Linden 12;
Telephone: 420019; Teleprinter: Berlin 1188;
Cables: Technikverlag Berlin.

Production: Druckerei der Werktätigen, Halle (Saale),
Kleiner Berlin 1a

Published under Licence-No. 2132 of the German Democratic Republic.

Monthly Technical Review

Published by VEB Verlag Technik

Chief Editor: *M. Kühn*

Volume 1, No. 10 Berlin December 1957

THE KEY

Machine building is rightly called the heart of a country's economy; all other branches of industry depend on it for their further development. The sooner the machine building industry of the German Democratic Republic succeeds in developing and producing machines and aggregates of still higher perfection, the sooner all other industries will be able to satisfy the requirements of this and other countries.

Great Tasks

The main tasks set for the industry of the GDR by the Second Five-Year Plan are the rapid development of energy production, the raising of soft coal mining, greater output of building materials, and the development of some branches of the chemical industries. All this means higher demands on our machine building industry. In addition, there is a constantly increasing demand for complex machines required by the fast growing sector of our socialist agriculture. (see, e. g., Steffen, The Tool-Carrier RS 09, pp. 257 and 258 of this volume).

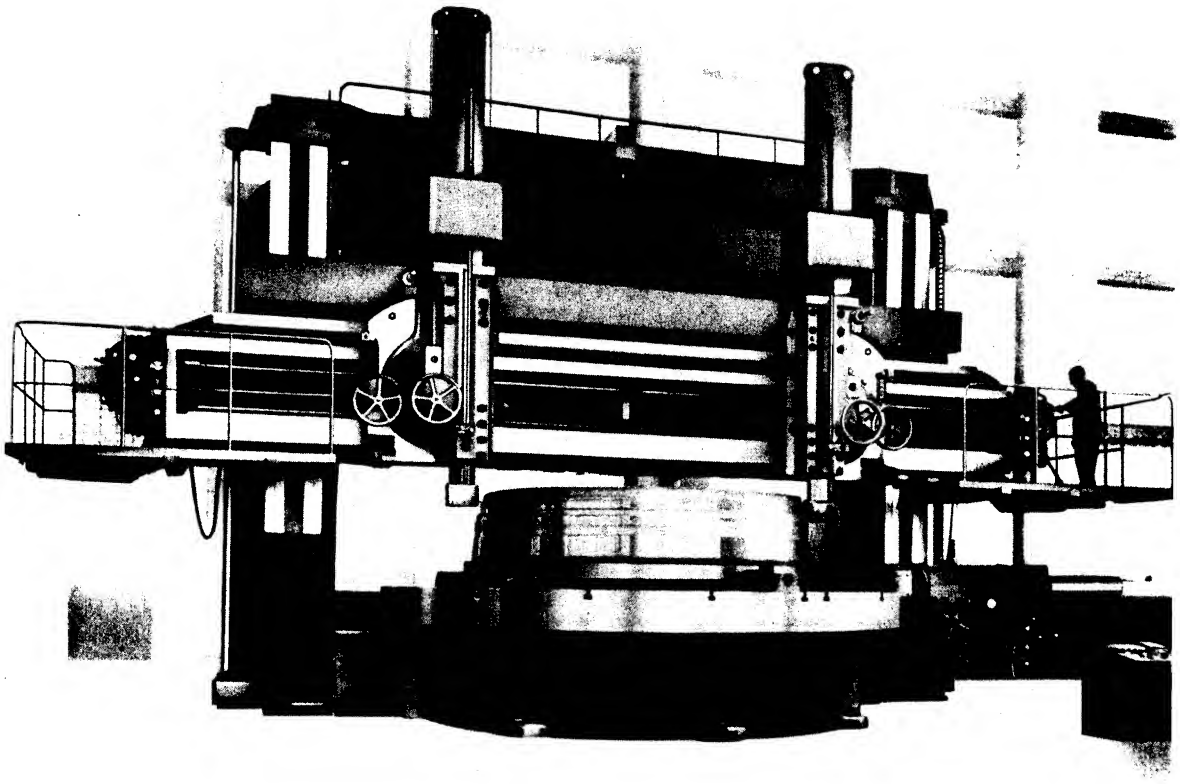

Fig. 1. Double column vertical boring mill Model DKZS 6300 × 2500 (Manufacturers: VEB Großdrehmaschinenbau "7. Oktober", Berlin-Weißensee)

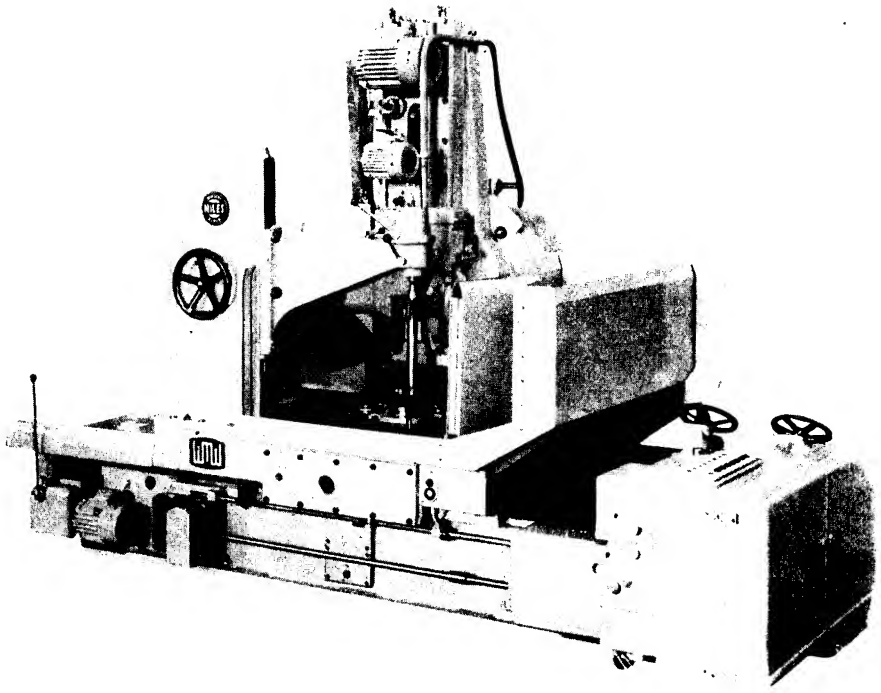

Fig. 2
Spur gear grinder (generating method) (Manufacturers VEB Großdrehmaschinenbau "7. Oktober", Berlin-Weißensee)

Great Accomplishments

Our machine building enterprises are working arduously to further the production of highclass machines. Only a short time ago the wire rope spinning machine 48 DVM 1000 was completed by VEB Schwermaschinenbau Ernst Thälmann, Magdeburg. With a total weight of 370 t and an overall length of 65 m, it is the largest machine of its kind built up till now.

Out of the large group of well-known trade marks only WMW may be mentioned. These three letters signify top products of our peoples'-owned machine tool building industry; many of these have become known on the world market. In our previous issues we have acquainted Monthly Technical Review readers with some of these machines (see Vol. 1 No. 1, pp. 3 – 7, New Developments in the Lathe Building Industry at the Technical Fair Leipzig 1957; pp. 8 – 10, Haupt, Vacuum Forming of Thermo-Plastics; No. 2, pp. 27 – 32, Willeke, Gauge-Controlled Grinding Machines; No. 3, pp. 55 – 58, Masthoff, Planing Machines; No. 4, pp. 81 – 86, Schröder, Trends in the Development of Gear Cutting Machines).

Those who know the quality and the capacity of the machines built in the German Democratic Republic will ask themselves how such top-performances were possible.

Many Years of Production-Experience.

The above-mentioned WMW enterprise in Magdeburg has begun to build rope spinning machines as far back as 1892. There is no doubt that this decade-long experience has its beneficial effects on the capacity and reliability of these aggregates.

Raising a New Generation of Technicians

There are 21 specialized Colleges with 13200 enrolled students alone in the field of machine building in the German Democratic Republic. In addition, roughly 15000 internal and 3600 external students are trained in the technical sciences in our Technical Colleges and Universities.

Generous Support of Technical Research

Large sums are put yearly at the disposal of our research workers by the People's Government. An extensive research program is being carried through in the industrial and scientific research laboratories, among them the Institutes of the Technical University at Dresden, staffed with a large number of highly qualified experts working in close connection with the industry; (we have reported for instance about the tasks and work of the Central Institute of Welding Technique, Halle (Saale), in the contribution by Dr. Gilde, Welding in the German Democratic Republic, Vol. 1, No. 7, pp. 149 – 152).

We should like to remind our readers of the series of reports about the results of the research work carried out in the Institute for Applied Fluid Dynamics of the Technical University, Dresden (Director: Prof. Dr.-Ing. W. Albring). (Cf. also: Pascher, Experimental Determination of the Lines of Constant Speed in the Field of Hydrodynamic Guide Grids by Means of Soap Skin Models, pp. 235 – 240, this issue).

Cooperation between Technicians and Scientists

The Kammer der Technik, the organization of engineering scientists and technicians, has contributed largely toward technical advancement during the ten years of its existence. The results of the group Machine Building are among the most important ones.

The Key

Thus, the acknowledged quality of the GDR machine building has many causes. Workers, engineers, and scientists of our people's-owned enterprises will not cease in their efforts to consolidate this fame and to produce still better and more perfect machines in the future.

Experimental Determination of the Lines of Constant Speed in the Field of Hydrodynamic Guide Grids by Means of Soap Skin Models

By W. Pascher, Dipl.-Ing., Dresden [1])

Communication from the Institute for Applied Fluid Dynamics of the Technical University Dresden – Director: Prof. Dr.-Ing. W. Albring

The calculation of potential flow through strongly deflecting guide grids is difficult and time consuming. An optical method based on the soap skin-flow analogy has been developed for rapid determination of lines of constant speed. It is possible to photograph the soap skin with a comparatively simple camera in such a way that the photograph will show directly the lines of constant speed. These photos will facilitate the selection of advantageous shapes of profiles.

Contents

1. Introduction

Guide grids for the deflection of flowing liquid or gas play an important part in many technical applications. The capacity and efficiency of a machine or installation depends very often on the quality of its guide grids. To determine the shape of these grids by theoretical calculation is extremely difficult and time consuming if a strong deflection of the flow is to be obtained. It has therefore become the custom to design these grids according to simple empirical rules which very often are out-dated. The experience made with already constructed grids is not sufficient to find the best profile in every new case.

The usual way of developing stream-line profiles is to investigate first the velocity distribution or the pressure distribution of the potential flow, and to account for the influence of viscosity by a subsequent correction based on boundary layer theory. A rather good judgement about the suitability of a given profile can however in most cases be given already on the basis of the theoretical pressure distribution according to potential theory. Yet for strongly deflecting grids it will be difficult to calculate the potential flow, i. e., to adapt the known solutions of the differential equation to the boundary conditions of the grid.

A possibility to solve such problems in a convenient way is given by using models. This means that another physical phenomenon is used which complies with the same differential

[1]) Paper read at the 1st Polytechnic Conference held at the T. U. Dresden on June 19th, 1956. Translation of the German publication in Maschinenbautechnik Vol. 5 (1956) No. 12 pp. 662–667.

The Soap Skin Analogy

Plane field of flow	Soap skin
Flow function ψ	Vertical coordinate z
Differential equation $\frac{\partial^2\psi}{\partial x^2}+\frac{\partial^2\psi}{\partial y^2}=0$	Differential equation (for $\varphi \ll 0$) $\frac{\partial^2 z}{\partial x^2}+\frac{\partial^2 z}{\partial y^2}=0$
Quantity of flux $\Delta\psi$	Difference of height Δz
Velocity: $\frac{\partial\psi}{\partial y}=w_x$	Inclination: $\frac{\partial z}{\partial y}=\tan\varphi_{(y)}$
$\frac{\partial\psi}{\partial x}=w_y$	$\frac{\partial z}{\partial x}=\tan\varphi_{(x)}$
$\frac{\partial\psi}{\partial n}=w$	$\frac{\partial z}{\partial n}=\tan\varphi$
w_∞	$\tan\varphi_\infty$
Rigid wall, stream line $\psi=$ const.	Plane edge, line of height $z=$ const.
Level from which the parallel flow with normal component $K\cdot w_\infty$ emerges	Slanted straight edge piece with angle of inclination φ
$\frac{\partial\psi}{\partial s}=K\cdot w_\infty$	$\tan\varphi=K\cdot\tan\varphi_\infty$

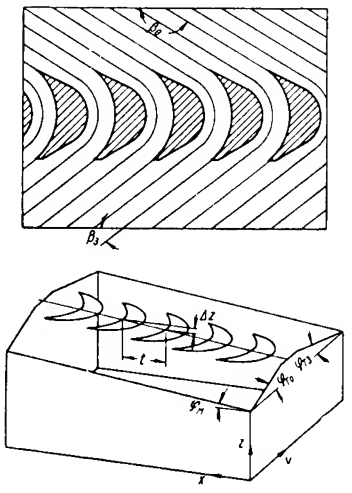

Fig. 1. Analogy between flow function and soap skin

equation. One only has to transpose the original boundary conditions to the model. Furthermore the function appearing as the solution should be capable of easy accurate evaluation.

2. The Soap Skin Model

I have used the soap skin model. The vertical coordinate z of a stretched soap skin satisfies approximately the potential equation $\Delta z = 0$ if the skin is only slightly inclined against

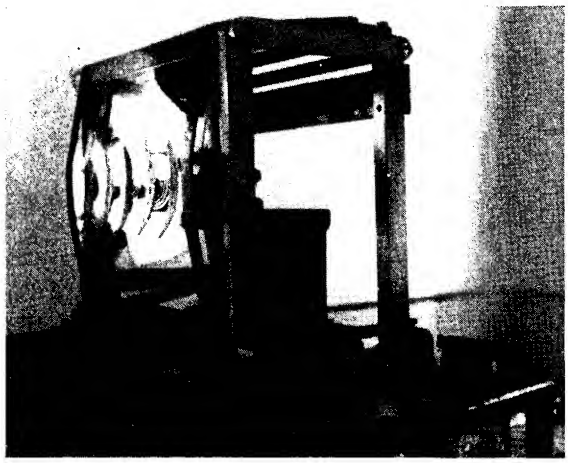

Fig. 2. Model of a guide grid flow, with skin

the x-y-plane. The vertical coordinate z of a stretched soap skin can thus be considered as corresponding to the flow function ψ which complies with the same differential equation $\Delta \psi = 0$.

The analogy between soap skin and potential flow is explained in detail in Fig. 1. The differential equations are the same in both cases. The difference of height between two points on the soap skin corresponds to a certain amount of flow between these points. The direction of flow in a given point corresponds to a line of equal height through the corresponding point of the skin. The inclination of the soap skin corresponds to the flow velocity.

Each stream-line corresponds thus to a line of equal height on the skin. Since the profile is also supposed to be a stream-line, the corresponding line of equal height must be enforced in the model. This is done by using in the model metal sheet disks with sharp edges arranged parallel to the x-y-plane. All other boundary conditions will be realized so far away from the model proper that the conditions practically will correspond to parallel flow. Straight frame parts will be used there, the inclination $\tan \eta$ of which will be proportional to the normal component of the flow vector.

A clear idea of the soap skin model may be gained by drawing the field of the stream lines and then considering them as lines of equal height.

Fig. 1 shows the flow through a grid of guide blades with the stream lines clearly indicated. In front of and behind the grid the stream lines are parallel; hence the corresponding soap skin is plane and inclined correspondingly. Below this drawing the angles of inclination have been drawn in a perspective presentation. Tangens η_M corresponds to the normal component of the flow through the grid, which is the same in front of and behind the grid. Tan η_T represents the velocity component parallel to the grid, which will change with the passage of the fluid through the grid. The difference of height Δz of two neighbouring profiles fixes the quantity of flux between them and must conform to the angle η_M.

Fig. 2 shows the apparatus by means of which we have realized the boundary conditions of the grid. The models are seen in the middle. From them to the frame the soap skin is stretched. The sides of the frame are made of rubber and can be adjusted to the desired angle. Of the skin only reflections are seen, about which it will be said more further on.

Fig. 3 shows the same apparatus without the soap skin. The adjusting devices are therefore better visible. The models are bolted in a perforated ledge and can be turned round. With this arrangement the grid division constant and the grading angle of the series of models can easily be changed. Differences in height are obtained by bolts of different length.

The whole frame is fastened to a basic plate which can be slanted according to the grading of height of the guide grid. The upper and the lower half of the frame can be slanted normally to this by micrometer screws. The inclination $\tan \eta_T$ can be read off directly from these screws; it corresponds to the velocity component parallel to the guide grid. Both halves of the frame can also be displaced parallel to each other. There is furthermore a dish for the soap solution, fixed to the lower side of the frame. The soap skin is produced by immersing a flexible strip of plastic material into the solution and drawing

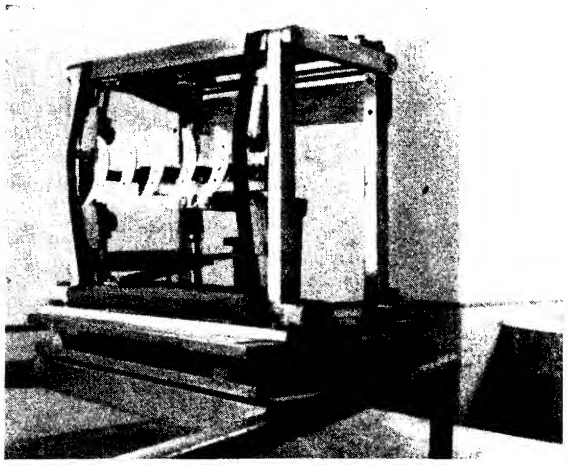

Fig. 3. Model of a guide grid flow, without skin

it upwards over the frame. The skin must adhere immediately to the models and the strip of plastic material must be pressed well against the wall of the frame, especially when drawing it off.

In order to represent in the model a certain condition of flow, the models are first screwed on and adjusted. Now the frame plate is turned into the direction of the models and is adjusted to the desired inclination by the micrometer screws. This inclination is calculated from the given grading of height and the angle of inflow or outflow. Next the soap skin is drawn and both parts of the frame are displaced parallel to each other till the skin shows an equal image on all models and a stagnation point appears at the rear edge, i. e., till the rear edge of the model is even with the surrounding soap skin. This can be judged best by sight.

It is impossible to comply with the stagnation point condition so accurately that small differences between β_2 and β_3

can be recognized and corrected. Yet the distribution of velocity will be noticeably influenced by this inexactness only in the immediate proximity of the rear edge. The frame will therefore be adjusted to β_2 on the outflow side and will be left there.

The soap solution of water, natriumoleate, and glycerine, prepared according to *Boys* [1], will produce skins which will last 3—4 tests of about 2 minutes each.

Something must still be said about the errors of the soap skin analogy. The soap skin analogy holds only approximately. The differential equation of the soap skin coincides with the potential equation only when the inclination η is small compared to 1. Most, authors refer in this connection to an estimation of error given by *Griffith* and *Taylor*, which we could not obtain. According to this estimation angles of up to 30 degrees are permissible. Yet we have found that the values c_a measured by us are too high by 6—8 percent as compared to the theoretical values given by the conservation of momentum. This fault is caused by the approximation character of the soap skin analogy and is a systematic deviation which however will limit the usability of the results only insignificantly because the velocity distribution will be maintained qualitatively.

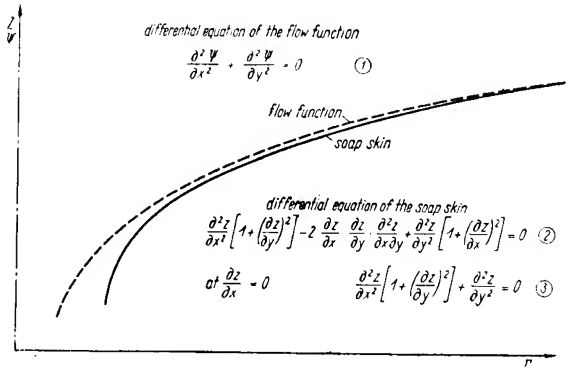

Fig. 4. Errors of the soap skin analogy

In Fig. 4, equ. (2) the exact differential equation of the soap skin is noted down. If the system of coordinates is rotated in such a way, that the x-axis becomes tangential to a line of equal heights, we receive $dz/dx = 0$ and hence equ. (3), from which it can be seen that the 2nd derivative along the line of descend will always be higher in the x-y-direction than normal to this. Both differential quotients will be equal for potential surfaces. The soap skin is therefore too strongly curved normally to the contour, so that the angles of inclination, and hence the velocities, will come out too large on the suction side and too low on the pressure side, if the boundary conditions are correctly represented. For small values of $\left(\frac{\partial z}{\partial x}\right)^2 \sim 0$ and $\left(\frac{\partial z}{\partial y}\right)^2 \sim 0$, equ. (2) will be transformed into equ. (1). For reasons of comparison we have drawn in Fig. 4 the axial section of the flow function and the soap skin function of a potential whirl. By means of these functions we have also verified the errors numerically and here found the expected values.

3. Evaluation of the Skin Shape

The use of a model is only sensible if the model can be evaluated comparatively easily. In previous investigations the procedures used were either mechanical or optical. The optical method has the advantage that the skin will not be influenced by it. The stereoscopic evaluation, for example, belongs to this class, but in this case the skin must first be made visible as otherwise it will not be seen on a photograph. It is better to take advantage of the skin's capacity for reflection and to measure its angle of inclination in certain places [7]. One can dispense with the graphic differentiation of the field of flow when measuring the angle of inclination because when investigating a field of flow one will be interested not in the numerical values of the flow function but practically only in the velocities, which are proportional to the angle of inclination.

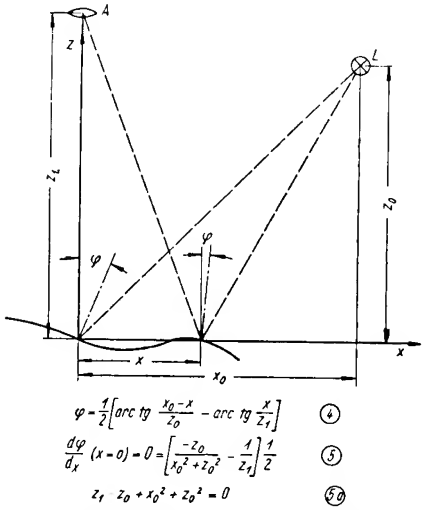

Fig. 5. Measurement of skin inclination by reflection

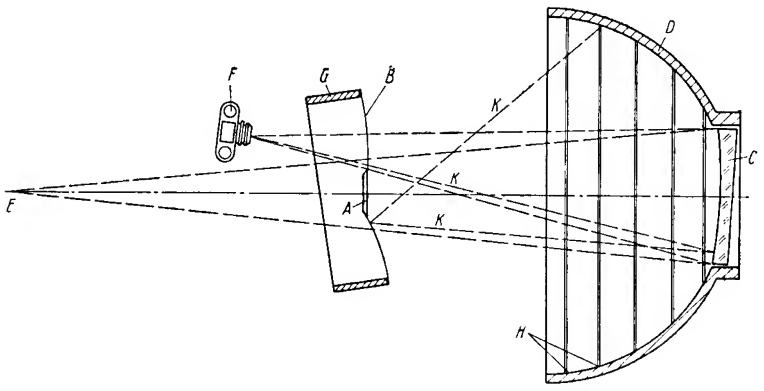

Fig. 6. Test stand diagram
A model – B soap skin – C concave mirror – D spherical shell – H source of light, corresponds to c/c_∞ – const. (white ring on black background) – F camera – G frame for soap skin – E intersection of the rays falling on the objective of the camera – K path of a light ray

A simple measuring arrangement for measuring the angles of inclination can be seen in Fig. 5. The skin is observed vertically from above (A), and when the image of a light source can be seen at zero the angle of inclination of the skin at that point will just be $\eta = {}^1/_2 \arctan x_0/z_0$. we have also written down the

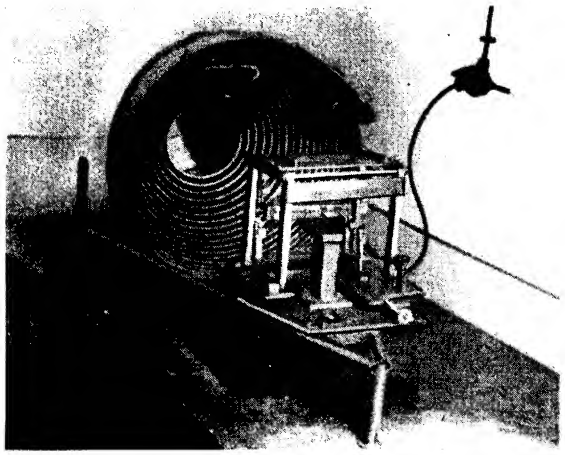

Fig. 7. Test stand, seen from the model side

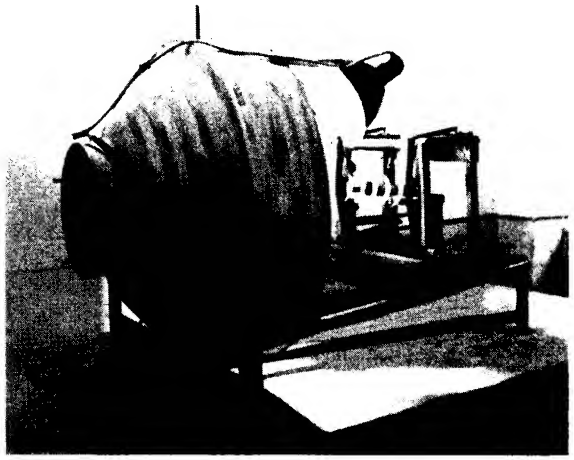

Fig. 8. Test stand, seen from the shell side

angle of inclination for the case that the point observed does not lie vertically below the eye [equ. (4)]. The variation of η at constant source of light is an error of first order. In order to keep it reduced to acceptable dimensions a distance of 5 meters should be used for an image field of 5 mm, or else the rays should be made parallel. It is also possible to correct the error approximately. In order to do so we have calculated the measured angle in a general way [equ. (4)] and have placed the derivative $d\eta/dx = 0$ at $x = 0$. Then the measured angle will be an extremum in this point and the error will be compensated in the first approximation.

As can be seen from equ. (5), z_1 must always be negative. This can be realized by using a large lens or a concave mirror. All rays which seem to come from the same point beyond the soap skin are collected by these devices and then directed towards the eye or the photographic objective. The main advantage of this arrangement is the fact that now all points on the soap skin can be obtained which are inclined by the same angle η but are not necessarily located in the same plane. In this case the source of light should be enlarged to the shape of a closed luminous ring. Changing the optic adjustment is not necessary. If the source of light is now reflected by all points inclined by η, the image formed by reflection will be an isocline (line of equal inclination) of the soap skin, or an isotache (line of equal velocity) of the analogue field of flow. In order to find out the position of other possible sources of light that would also produce isotaches with the same optic arrangement we put $z_1 - x_0 = 2R = \text{const}$ and obtain the vertex equation of a circle for the relation between z_0 and x_0 equ. (5). The ring-shaped sources of light are therefore all located on the surface of a sphere formed by rotating the first circle about the z-axis.

Fig. 6 shows the diagram of the test stand constructed in this way, with the path of a light ray drawn in. The camera points through the skin to the concave mirror. In order to reduce aberrations the angle between camera normal and mirror normal should be as small as possible. This angle gives rise to astigmatic errors which will grow with the sqare of the angle. The test stand was constructed with a spherical mirror of 300 mm radius and operates with an accuracy of about 1

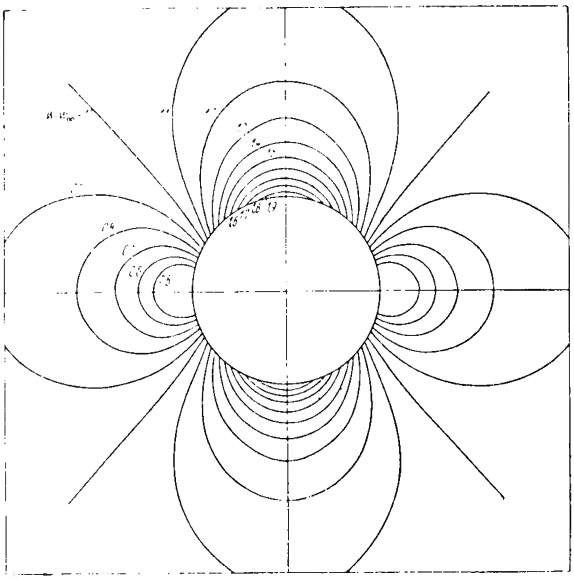

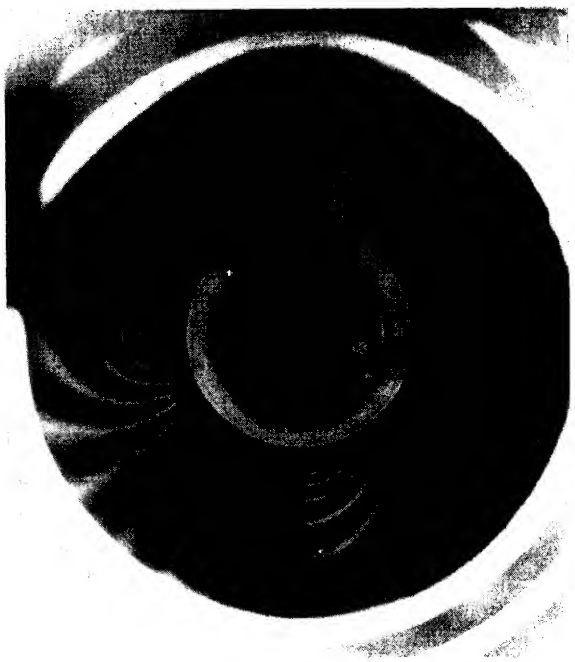

Fig. 9a and b. Picture of isotaches for flow around a cylinder
a) Theoretical curves b) Measured curves

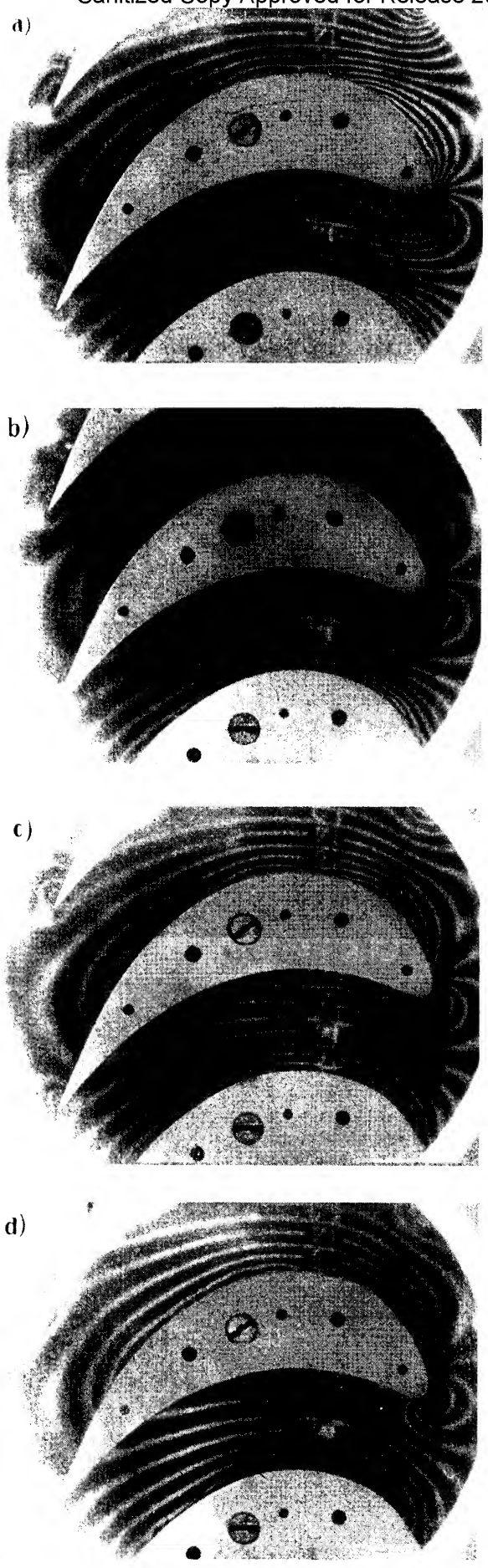

percent of the quantity to be measured (i. e., tan η) when the diameter of the image field is 100 mm. Directly at the model the error is somewhat smaller. As no sources of light can be located at the place of the mirror the smallest measurable angle of inclination is 5 degrees. Figs. 7 and 8 show two views of the ready test stand; the arrangement of the mirror and of the ring-shaped light sources can be seen clearly in Fig. 7. The sources of light are white rings on the otherwise black concave side of spherical shell illuminated by two 200 W lamps. The individual rings are numbered in mirror writing so that these numbers are seen correctly in the mirror, thus facilitating the evaluation. The model as well as the holding and adjusting devices for the concave mirror can be seen in Fig. 8.

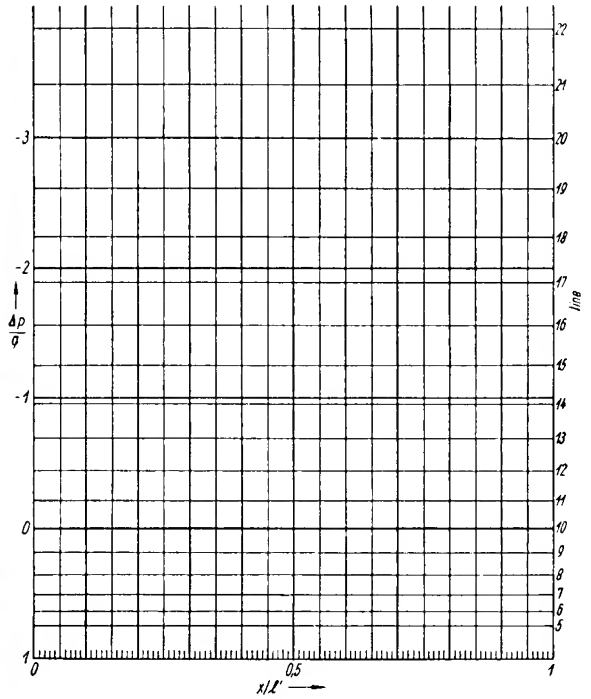

Fig. 11. Evaluation sheet

4. Test Results

The photograph of the model of a circulation-free flow around a cylinder is shown in Fig. 9 to the right, while to the left curves calculated from potential theory are drawn. A comparison of both pictures will show clearly the applicability of the model and the method used.

The surroundings of the stagnation points around which the isotaches close in almost circular curves are typical. Similar pictures result also at the nose of single and grid profiles.

A series of grid photographs corresponding to different angles of influx are shown in Fig. 10. The variation of this angle has a noticeable effect only at the front part of the profile. The profile was developed by us by superimposing a drop and a curved skeleton line. The disturbances on the surface of the profile are caused by small faults in the sharpened edge. The lines become a bit indistinct at the rear edge because the skin cannot represent the sharp changes of velocity immediately at the edge.

The velocity distribution on the pressure side is quite

Fig. 10a—d. Pictures of Isotaches of guide grid flow for different angles of influx. $t/l' = 0.53$; $\beta_3 = 30$ degrees
a $\beta_0 = 155$ degrees c $\beta_0 = 145$ degrees
b $\beta_0 = 150$ degrees d $\beta_0 = 140$ degrees

favourable. The flow is accelerated almost along the whole stretch, so that there is no danger of the boundary layer becoming detached. The picture is not so favourable on the backside because there the flow is retarded already rather near the front. The danger of boundary layer detachment would therefore exist. The course on either side of the retardation point (at $\beta_0 = 150$ degrees) is comparatively favourable, the speed being constant and the pressure increasing further on. This region of retardation could be avoided by correcting the shape of the profile.

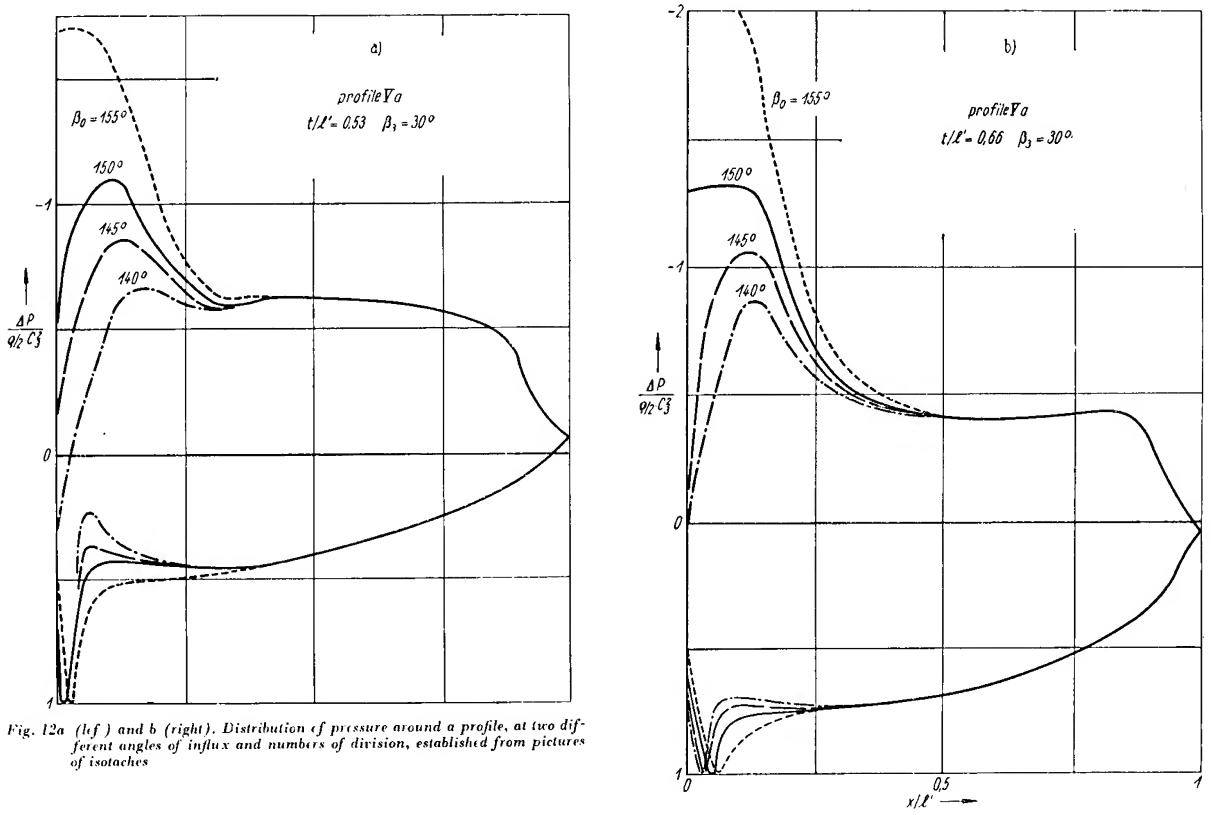

Fig. 12a (left) and b (right). Distribution of pressure around a profile, at two different angles of influx and numbers of division, established from pictures of isotaches

An even distribution of velocity on the suction side is of special value for profiles destined for steam or gas turbines because the flow velocity will here often reach values comparable to the speed of sound. If there are any places with a high velocity on the suction side, the speed of sound can easily be surpassed. This would cause additional losses and an increased danger of boundary layer detachment.

The photographs are evaluated on a ruled sheet of paper as shown in Fig. 11. For each line of the photograph $\Delta p/q$ was calculated and the value found was marked on the sheet. The photograph of isotaches is projected on square paper for purposes of evaluation. The negative of the photograph can be used for this purpose. Then the distance between the beginning of each line and the front edge is measured and a point is marked on the sheet at the point x/l' on the corresponding horizontal line. These points are then joined by a curve which gives the distribution of pressure.

The result of such an evaluation is represented in Fig. 12. It is the distribution of pressure for two profile grids of different divisions and different influx angles. The variation of the influx angle makes little difference at these grids with small divisions, the outflux remaining practically unchanged. We want to point once more to the corner at $\beta_0 = 150$ degrees in the pressure distribution which indicates a fault of the profile and which will become an underpressure point at a steeper influx ($\beta_0 < 150$ degrees).

If it should be possible to compensate this corner, the drive-up value of the grid and with it the number of divisions could be increased without increasing the maximum speed.

5. Summary

We wish to summarize the main points of guide grid investigation by means of soap skin models. For the investigation of the grid we need a set of very accurate models. Of special importance are plain surfaces and smooth and sharp edges. The flow function of the potential flow is represented by these models in the test stand described above and lines of equal speed are photographed. It is possible to vary influx angle, grading angle, and division. The field of isotaches allows to judge the qualities of the profile and indicates the points at which the profile may still be improved. This procedure is specially suited in cases where large differences of velocity will appear, i. e., for large angles of deflection. It will be the aim of further investigations with this apparatus to determine the parameters of the most suitable grid shapes in dependence on the angles of flow. TRA 87

Literature

[1] *Boys, C. V.:* Seifenblasen. Leipzig 1913.
[2] *Quest, H.:* Eine experimentelle Lösung des Torsionsproblems. Ing.-Archiv Vol. 4 (1933) p. 310.
[3] *Funke, W.:* Bestimmung des Auftriebes von Tragflügeln mit Hilfe des Prandtlschen Membrangleichnisses. Dissertation Hannover 1938.
[4] *Biezeno-Grammel:* Technische Dynamik. 2nd Edition Berlin 1953.
[5] *Bauersfeld:* Über eine Erweiterung des Prandtlschen Membrangleichnisses. Ing.-Archiv Vol. 5 (1934) p. 69.
[6] *Thiel:* Photogrammetrisches Verfahren zur Lösung von Torsionsaufgaben. Ing.-Archiv Vol. 5 (1934) p. 417.
[7] *Reichenbächer:* Selbsttätige Ausmessung von Seifenhautmodellen. Ing.-Archiv Vol. 7 (1936) p. 257.

A Simple Geometric Construction to Replace the Adiabatic Ellipse in the Construction of Mach Lines

By K. SCHIEFERDECKER, Dipl.-Ing., Dresden [1])

The behaviour of laminar plane supersonic flows can be theoretically comprehended by the method of characteristics due to *Prandtl* and *Busemann* [1].

For an ideal gas the characteristics in a polar diagram $M^*(\delta)$ follow as congruent and reflected epicycloidal arcs which result one from another by rotating through the multiple of a fixed angle.

Here,

$M^* = c/a^*$, the critical velocity ratio (Mach number) at the point observed, and

$\delta =$ the angle between the flow directions in two successive points of the field of flow.

construction of the epicycloids can be applied with advantage.

Let us construct the Mach line through the point A, (Fig. 1), of the solution characteristic. The circular arc about A with radius r (radius of the rolling circle k) intersects the circle k_1, on which the center of the rolling circle is moving, in point B. $\overline{EO}$ intersects the base circle K in point P, the instantaneous center of rotation of the two generating circles (planes).

$\overline{PA}$ is perpendicular to the trajectory and in the direction of the Mach line. Since the circle k_1 is supposed to be given the construction merely consists in describing a circular arc and in drawing two straight lines.

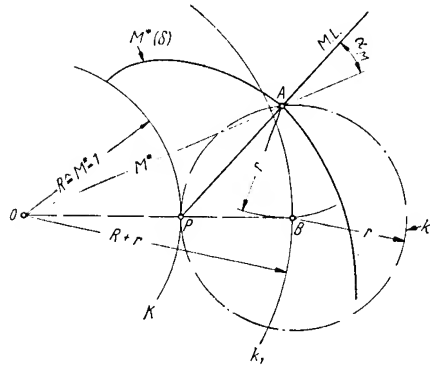

Fig. 1. Construction of the Mach line as normal to the solution epicycloid $M^*(\delta)$ in the diagram of characteristics

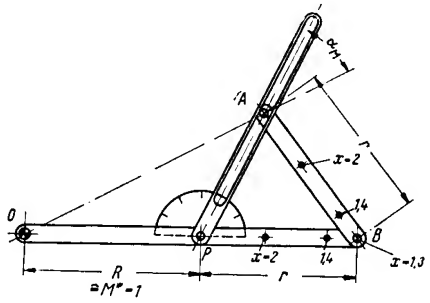

Fig. 2. (right) Instrument for drawing normals in the diagram of characteristics

Particular importance attaches to the normal to the characteristic in the point of solution. As Mach line, it connects points of constant flow condition (constant velocity, pressure, density, and temperature). The well-known text books of fluid dynamics describe the determination of the Mach line from the diagram of the characteristics by means of the adiabatic ellipse. This determination, though theoretically correct, is unpractical. The working with a template (adiabatic ellipse) is not an exact construction in sense of classical geometry. As the characteristics are epicycloidal arcs, the known normal

For frequent application the construction illustrated in Fig. 2 is recommended.

Let $R \triangleq M^* = 1$, $r/R = \frac{1}{2}\left(\sqrt{\frac{x+1}{x-1}} - 1\right)$,

and 0 being the origin of the diagram; then $\overline{AP}$ is the normal to the solution curve and in the direction of the Mach line.

For $x = 1.30 \quad 1.405 \quad 2$

we have $r/R = 0.8844 \quad 0.71814 \quad 0.3660.$

TRA 85

[1]) Communication from the Institute for Applied Fluid Dynamics of the Technische Hochschule (Technical University), Dresden. Director: Prof. Dr.-Ing. *W. Albring*. Translation of the German Publication in Maschinenbautechnik Vol. 6 (1957) No. 3 p. 171.

Literature

[1] *Sauer, R.:* Einführung in die theoretische Gasdynamik. Springer-Verlag 1951, p. 40, pp. 64–66, pp. 119 etc.

Thickness Measurements of Oil Films

By Prof. Dr. A. Dierichs and H. Gabbert, Freiberg/Saxony [1])

Communication from the Institute for Organic Chemistry and the Chemistry of Coal and Oil, Bergakademie Freiberg
Director:
Prof. Dr. A. Dierichs

It is possible to-day to determine the general structural characteristics of lubricants, by chemical, physical, and electrophysical analyses, but it is still impossible to predict with certainty the lubricating properties by such analyses. In general, predictions of this type can be made only on the basis of actual tests with the machines to be lubricated, particularly where the lubricants are subjected to very high operating pressures.

After, in 1952, Ubbelohde [1] had introduced a new characteristic property called by him "statische Tragfähigkeit" ("static bearing strength"), the Institute for Organic Chemistry and the Chemistry of Coal and Oil at the Bergakademie Freiberg begun a series of investigations on this subject.

Starting from the observation that mercury placed between two differently curved watch glasses can be expelled from the zone of contact by sufficiently high static pressure while this is impossible in the case of lubricating oils, *Ubbelohde* was led to the conclusion that the molecular layers of an oil film adhering to a surface within the range of the adsorptive forces of such solid surfaces are able under pressure to adopt the character of a solid substance and, accordingly, a definite, measurable thickness. In contrast to all known mechanical oil-testing methods, this definite thickness is measurable in absolute units.

The measurement of the "static bearing strength", i. e., the determination of the *thickness-pressure function*, of an oil film leads to index numbers of great practical importance since it deals only with the layer of the lubricating agent remaining between the solid surfaces under pressure and thus excludes the influence of hydrodynamical processes that complicate the evaluation of other tests and measurements. The ideal condition is approached in sleeve bearings rotating at low speed within the range of limiting friction. The adhering oil film between the two surfaces may then be considered a protective layer preventing the creation of dry friction between the two metallic surfaces. From this it might be expected that the lubricating capacity of an oil increases with the thickness of this protective layer.

1. Determination of Thickness-Pressure Functions

The experimental determination of thickness-pressure functions requires the following apparatuses:

1.1 Interference comparator
1.2 Pressure apparatus
1.3 Measuring plates.

1.1 The Interference Comparator

The interference comparator (Inko) designed and constructed by VEB Carl Zeiss Jena permits measurements to be carried out with the monochromatic light of helium and krypton lines.

The Inko-apparatus consists of three main sections: the monochromator, the interferometer, and the telescope. All parts are rigidly connected with each other and are located in a casing provided with suitable heat insulation.

The monochromator is composed of the helium or krypton tube, the condenser, the collimator with entry slit and objective, and the dispersing prism. The interferometer consists of two glass wedges, the reference mirror, and the object plate, while the main parts of the telescope are the telescope objective, the exit slit, and the eye-piece. The interference pattern is made up of light and dark interference bands observed through the telescope. Well-measurable interference bands are produced only when all optical surfaces are highly polished so that the surface roughness falls below 0.1 μ.

1.11 Measuring Procedure

Using monochromatic light interference bands are produced on the surface of the object to be measured as well as

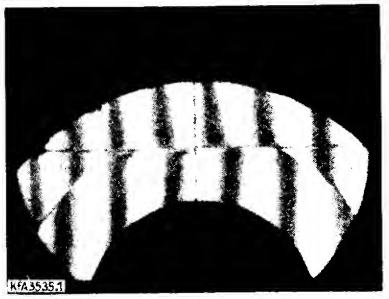

Fig. 1. Interference bands on object and pressure plate

on the object plate supporting the body. The telescope shows two band systems side by side (Fig. 1), the distance between two consecutive dark bands corresponding to half a wave length $\lambda/2$. The band displacement towards the left is now estimated in units of $\lambda/2$. (According to Fig. 1, this value amounts to 0.3). Since a single measurement would lead to inaccurate results, the estimated values were determined twice for all spectral lines used, i. e., for red, yellow, green, blue-green, blue, and violet. Since measurements were only carried out to heights of up to 25 mm, only spectral lines of helium were used in these tests, i. e.,

Red	with wave lengths of	0.6678184 μ
Yellow		0.5875649 μ
Green		0.5015702 μ
Blue-green		0.4921955 μ
Blue		0.4713168 μ
Violet		0.4471501 μ

[1]) Translation of the German Publication in Kraftfahrzeugtechnik Vol. 7 (1957) No. 6 pp. 210—212 and No. 7 pp. 251—253.

Evaluation was effected in accordance with the following equation: –

$$L = \frac{x\,\lambda}{2} + n\,\frac{\lambda}{2}.$$

L = the height of the object investigated,
x = the still unknown full number of wave lengths,
$\lambda/2$ = the distance between the bands, and
n = the fraction of the band distance.

The calculations were carried out with the aid of tables and light wave slide rules supplied by VEB Carl Zeiss Jena. The results obtained were corrected so as to refer to the meteorological standard conditions – 760 mm Hg atmospheric pressure – 10 mm Hg-vapour pressure at 20° C and NN. The corrections for the changes of wave length induced by the influence of air pressure, temperature, and atmospheric humidity were made according to the following formula:

$$c_2 = -0.36\,(b - 760) + 0.93\,(t - 20) + 0.05\,(e - 10).$$

These corrections may become quite large. It is therefore necessary to provide for thermostatic arrangements designed to restrict temperature variations to within ± 1° C, at a room temperature of + 20° C. This important provision was not fulfilled in the work described in the publication cited above.

1.2 The Pressure Apparatus

The pressure apparatus employed by *Ubbelohde* is unknown. The publication merely indicates that this apparatus remained outside the testing apparatus proper. The pressure apparatus developed for our investigations (Fig. 2) is a hydraulic pressure system in which the measuring plates subjected to pressure are not removed from the apparatus but remain in the Inko for measuring purposes. The apparatus consists of the pressure cylinder equipped with two pressure gauges for the measurement of pressures up to 4 kg/cm² and up to 15 kg/cm², respectively. Within the cylinder, the pressure piston 1 together with the damping piston 2 moves against a glycerine filling. Rod 3, fastened in the damping piston, connects the pistons with the pressure nut 4 which acts through the pressure cone 5 on the pair of measuring plates 6. The pressure is created from outside by tightening the knurled pressure nut. The forces transmitted by the pressure cone act exactly normal to the contact surface of the pressure plate in order to avoid distortions of the measuring plates. The pressure piston has an effective area of 12 sq. cm., while the contact area of the measuring plates amounts to 6 sq. cm., resulting in a transmission ratio for the contact areas of 1 : 2. It is thus possible by manual actuation of the knurled pressure nut to obtain effective pressures of up to 30 kp/sq. cm.

1.3 Measuring Plates

The experiments without pressure were carried out with glass measuring plates supplied by VEB Carl Zeiss Jena and dimensioned similar to those used by *Ubbelohde*. Their contact areas measured 7.61 sq. cm. The steel plates were produced in our own workshops, with a contact area of 6.00 sq. cm. All measuring plates were brightly polished by VEB Carl Zeiss. The degree of surface roughness of the measuring and contact surfaces remained below 0.1 μ. The pressure plates were finished plane-parallel to 0.2 μ, at a diameter of 55 mm, while the plane-parallelity of the object plate need not be considered since only one of its surfaces is required for the measurement.

The values stated have to be considered minimum values for the degree of plane-parallelity and for the surface quality of the plates. The glass plates have been made of Jena-glass, Type FK 1, having a coefficient of linear expansion of 8.68 × 10^{-6}. The steel plates consist of hardened tool steel with a coefficient of linear expansion of 11.55 × 10^{-6}. The press ur plates are fitted with calottes (spherical indentations) for the oil.

2. Experimental Investigations

2.1 Preparation of the Measuring Plates

The most important prerequisite for accurate determinations is the exact measurement of the height of the pressure plate. This height, H_0, represents a constant for each individual pressure plate. Accurate measurements of H_0-values require perfect cleaning of the measuring plates. If these plates are not absolutely clean, it is impossible to effect perfect contact between pressure and object plate, while if the state of perfect cleanliness is attained the adherence of the plates to each other is so strong that they cannot be separated mechanically without damage. Cleaning of the measuring plates is effected with pure carbon tetrachloride and trichlorethylene. Other solvents have also been tried, of course, but had to be rejected after lengthy tests.

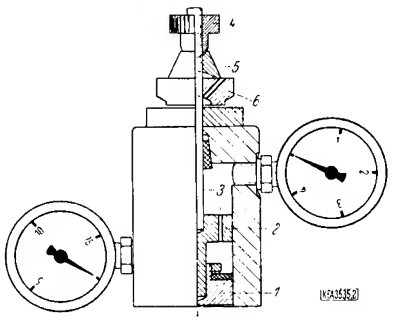

Fig. 2
Pressure apparatus

After preliminary cleaning the measuring plates were flushed with carbon tetrachloride and polished with a degreased piece of leather, followed by a second flushing with trichlorethylene. After complete evaporation of the solvent, the plates are rubbed down with clean linen or nettle cloth. Fibre remnants are brushed or picked off with a soft clean brush. The degree of purity of the plates can be tested by breathing on the surfaces before the second flushing treatment. If the uniform cloudiness induced by the condensing moisture of the breath is interrupted by darker spots, this indicates surface impurities which occur especially after previous measurements of oil films. Cleaning of the plates must therefore be repeated until the breathing film remains uniform over the whole surface. Trichlorethylene proved most satisfactory in this respect.

The cleaning process described above was applied in the same manner for glass and steel measuring plates, although the last and final proof of perfect preparation of the plates remains the attainment of perfect contact between the plates. This contact must apply to the entire contact area of the plates. The glass plates always exhibited isolated small cloudy areas indicating spots of unevenness on the contact surface. The control of the glass plates proved to be comparatively easy on account of the possibility of optical observation which is impossible in the case of metal plates.

2.2 Contacting and Separation of Measuring Plates

Contacting of the measuring plates was carried out only in the case of glass plates where the measurements of the oil films were performed without pressure, while contact treatment of steel plates was unnecessary on account of the forced

contact of the measuring plates under the load of the pressure apparatus. The reason for this difference in treatment is due to the different properties of the materials, especially to the strong tendency of steel to cold-welding. As pointed out by *Ubbelohde*, contacting of glass plates requires considerable experience in order to avoid erroneous measurements.

Glass plates are contacted by sliding the pressure plate on to the object plate from the side and turning it around (on the object plate) by slight pressure of the fingers. The circular interference bands produced by this motion have to be uniform in colour and width about the central point of the pressure plate. Very small pressure differences change the colour and width of the interference bands. When a uniform distribution of the bands has been obtained, the pressure on the rotating top plate is increased. Every change in pressure induces a corresponding change in the interference band system, i. e., the closer the plates approach each other, the wider are the bands produced.

Shortly before attaining perfect contact only the yellow bands remain visible, while complete disappearance of the interference bands indicates uniform contact of the plates over their entire contact surface. The last visible air film between the plates escapes rapidly at the moment of complete contact, the contacting plates remaining unclouded and clearly transparent.

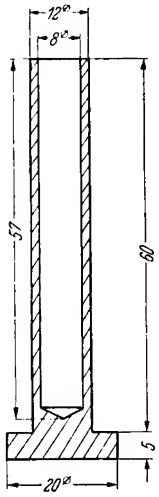

Fig. 3
Light-metal stamp for the separation of glass plates

In this condition, the H_0-value of the pressure plate is measured. If the appearance of the interference bands indicates one-sided contact of the plates, the contacting process has to be repeated. For this purpose it is necessary to separate the adhering part of the pressure plate, which requires considerable care and attention in order to protect the glass plates as they are easily damaged in the dry condition.

Separation of tightly adhering plates was effected by means of the light-metal stamp shown in Fig. 3. This stamp was heated to 80° C and placed on the pressure plate, heating the latter and inducing a small but sufficient thermic expansion of the plate material to effect automatic separation of the pressure plate from the object plate. This process is accompanied by the appearance of interference bands. As soon as these bands have reached the outer edge of the pressure plate, it can be lifted up without difficulty. The pressure plate must never be lifted off by lateral displacement or rotation, since this will usually lead to scratches in the contact areas.

2.3 Measuring of Thickness of Oil Films between Glass Plates

Measurements of the thickness of oil films were carried out without additional measuring plate loads, the only pressure exerted being the dead weight of the pressure plate itself. The specific load on the contact surfaces then amounts to 2.6 g/sq. cm.

The H_0-value of the pressure plate was determined as follows: – The primary measurement of the H_0-value (characteristic length) was carried out with an optimeter, against a dimensionally similar slip gauge, to a degree of accuracy of $\pm$ 1.0 μ. The pressure plate was then contacted with the object plate and the pair of plates placed into the Inko. The height of the pressure plate was measured after the temperature of the pair of plates had adapted itself to the room temperature of the Inko.

We then estimated the displacement of the bands produced by the pressure plate in fractions of the band distance for the six spectral colours of helium light (red, yellow, green, blue-green, blue and violet), first in the order from red to violet and then in the reverse order. Each of these colours possesses its own wave length, which also introduced a change of the band displacement in the two band systems. The fractions of the band displacement of each colour read off by us were averaged and translated into dimensions of length, the results thus obtained then being subjected to the necessary corrections.

According to the instructions for Inko-measurements, the individual μ-values should not deviate from their mean value by more than $\pm$ 0.025 μ. For an end measure gauge of 1000 mm, this gives a permissible error of $\pm$ 0.0025% of the end measure length. If the same tolerances were permitted in the case of thickness measurements of oil films, the percentage error would amount to $\pm$ 12.5% for an actual film thickness of 0.2 μ. Deviations of this magnitude would make any accurate classification of oils by thickness measurements of oil films practically impossible. In the work here described it was possible by very accurate measurements to keep the error down to $\pm$ 2.5%.

When the measured H_0-value of a pressure plate has been confirmed by control measurements, this value can be used for all thickness measurements of oil films. It was found that in spite of most careful finishing of the measuring plates differences in height along the periphery of the pressure plates amounted up to 0.1 μ, but these differences were eliminated by keeping the position of the measuring plates towards each other and in the Inko-apparatus accurately the same.

After attaining perfect contact between the glass plates, the calotte was filled from the outside with the oil to be measured. The oil could be introduced between the two plates only by lifting the pressure plate by means of the light-metal stamp shown in Fig. 3. This stamp is fitted with a control thermometer. It is initially heated to 110° C; after cooling down to 105° C it is quickly placed on the centre of the pressure plate and left there until its temperature has dropped to 90° C. The heating effect of the stamp induces a corresponding expansion to the pressure plate, lifting it off the object plate. The interference rings again observed indicated that the contact between the plates was not entirely broken at all points. The open spaces between the pressure and the object plate filled up with oil at a decreasing speed. The decrease in speed is due to the cooling of the pressure plate and to the corresponding tendency of the plate to return into its original position. This tendency is much enhanced by the fact mentioned above that the pressure plate had not been completely separated from the object plate in the first place, a ring of about 2 mm width along the periphery of the pressure plate remaining in contact with the object plate until they are finally separated by the action of the oil introduced between the two plates. The entire process was carried out in an exsiccator and lasted about three hours, terminating with the wetting of the entire contact area with oil. The appearance of the interference bands in the space between the plates permits a clear observation of the filling process. (In the case of unobstructed migration the oil penetrating into the opening between the plates spreads almost circularly. If the spreading proceeds in a strongly oval manner, it is advisable to repeat the cleaning of the plates in order to avoid erroneous measurements.)

We did not observe any emergence of oil from the contact area to the outside, in contrast to *Ubbelohde.*

The thickness measurement of the oil film took place 20 hours later. This period has also been determined by experiment: practical constancy of the conditions between the plates was reached only after this period of time, the growth of the thickness of the film then proceeding only at an extremely slow rate. Transport of the plates into the Inko was carried out with all possible care in order to prevent any relative movements tending to influence the oil between the plates. After a waiting period of one hour the film thickness was measured in the same manner as used for the determination of the H_0-value, the latter being deducted from the value determined, the difference representing the thickness of the oil film.

It is possible, of course, that errors of measurement may occur even if all the measuring instructions have been duly observed. Such errors may be due to a difference in weight of the pressure plates and a corresponding difference in the thickness of the oil film over the entire contact area. The following section of this publication will therefore contain only the results obtained with one and the same set of plates.

2.4 Results of the Pressure-less Measurement of Film Thicknesses on Glass Surfaces

The experiments described above were conducted with the following lubricating oils: –

1. Mineral oil 1 (mixed-basic)
2. Mineral oil 2 (mixed-basic)
3. Synthetic oil 1
4. Synthetic oil 2

Table 1. Analyses of the Oils Tested

Indication	Mineral oil		Synthetic oil	
	1	2	1	2
d_{20}	0.910	0.925	0.872	0.893
Flp. o. T. (°C)	243	222	220	212
CT [%]	0.55	2.22	0.18	0.17
NZ	0.12	0.33	0.09	0.05
VZ	0.25	0.48	0.18	0.33
n_D^{20}	1.5040	1.5140	1.4815	not measured
V_{50} [°E]	12.51	13.61	12.31	11.64
VI	2.45	2.87	1.72	1.86

Table 1 gives the results of the analyses of the oils tested. The film thicknesses of the oils mentioned were measured after a waiting period of 20 hours at room temperatures of 20° C ± 1° C yielding the following results:

1. Mineral oil 1 — Film thickness = 0.153 μ
2. Mineral oil 2 — Film thickness = 0.123 μ
3. Synthetic oil 1 — Film thickness = 0.094 μ
4. Synthetic oil 2 — Film thickness = 0.048 μ

A comparison of the results obtained indicates that the films of the mineral oils tested are thicker than the synthetic oil films. A comparison of the viscosities of the oils tested, on the other hand, does not offer any conclusions regarding possible connections between viscosity and film thickness. The same applies to possible connections between film thickness and Conradson-test.

In order to determinate the influence of pressure on the results of these measurements, tests were carried out with steel plates.

2.5 Measurements with Steel Plates

The measuring plates were prepared by treatment with solvents in the same manner as the glass measuring plates.

2.6 Determination of Pressure-Thickness Curves

Unlike glass plates, steel plates are not brought into close contact by hand. In order to attain the condition of perfect contact between the plates, required also for the determination of the H_0-value of the steel plates, these are mounted in the pressure apparatus where they are subjected to a pressure of about 16 kp/sq. cm. for one hour. When after this period of compression the plates are removed from the pressure apparatus, the plates are in complete contact with one another.

It was first attempted to carry out the H_0-measurements for steel plates in accordance with the directions issued by VEB Carl Zeiss Jena, for the measurements of parallel end gauges. According to these instructions, the steel pressure plate has to be contacted with a glass object plate. These attempts indicated, however, that in comparison with gauge blocks the relatively large contact areas of the pressure plates do not so easily make contact. After numerous vain attempts to develop a satisfactory method for this purpose the only obvious method to attain reproducible H_0-values was to carry out the measurements under increased pressure in the pressure apparatus. In order to avoid destruction on the perfect contact surfaces by cold-welding, the contacted plates were separated thermically in accordance with the method employed for glass plates, which proved to be absolutely free of cold-welds.

The process was carried out as follows:

The cleaned steel plates were mounted on the pressure apparatus, subjected to a pressure of 16 kp/sq. cm. and installed in the Inko. The measurement of the H_0-value took place after a waiting period of one hour. After measuring the H_0-value, the plates were separated.

In most instances this work cannot be carried out without soiling the measuring plates by finger impressions, requiring a subsequent cleaning treatment. The contact surfaces of both plates are then wetted with the oil, leaving a large excess of oil on the contact faces. In this condition the measuring plates are placed into the desiccator. After 20 hours of conditioning in the desiccator the plates are placed together without removing the oil and fastened in the pressure apparatus. The measuring plates are now subjected to the pressure exerted by the pressure apparatus, usually to a pressure of 2 kp/sq. cm. The aggregate is finally placed into the Inko under this pressure.

Measurements are commenced after one hour of conditioning, the temperature adjustment being controlled by a special thermometer fitted at the Inko. After readings of the band systems have been taken a preliminary evaluation of the values obtained is made so as to determine whether, and to what a degree, the μ-values determined remain within the permissible range of errors. If this is not the case, the readings have to be repeated. If the permissible range of errors has not been exceeded, the pressure apparatus is removed from the Inko only for the adjustment of the next higher pressure stage and for immediate replacement. This process is repeated until the maximum testing pressure has been attained.

In the experiments under discussion the pressures were always increased by steps of 1.0 kp/sq. cm. After reaching a certain pressure value characteristic for the particular type of oil, the thickness of the oil film did not decrease by any measureable amount. Measurements of film thicknesses at decreasing loads could not be carried out on account for the fact that it proved impossible to adjust the pressure stages so as to correspond to the increasing pressure stages.

If the values determined by the measurements at the various pressure stages are plotted the graph shows a charac-

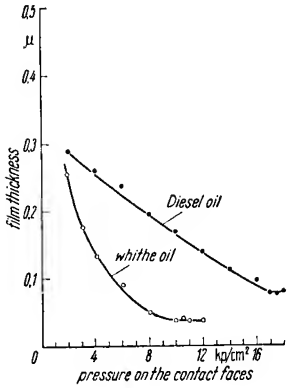

Fig. 4.
Measurement of film thickness of a Diesel oil and a white oil

Characteristic data	
White oil	
d_{20}	0.879
Flp. o. T. °C	208
CT %	0.013
NZ	0
VZ	0
V_{20} °E	16.52
V_{50} °E	3.65
VP	2.18
Diesel oil	
d_{20}	0.852
Flp. P. M.	65° C/728 mm Hg
Boiling characteristics acc. to ASTM	°C 189—321
V_{20} °E	1.53
V_{50} °E	1.13
Elementary analysis:	C = 86.60%
	W = 13.04%
	S = 0.10%

teristic picture of the decrease of film thickness with increasing pressure. The results of the experiments have been arranged according to the degree of viscosity as follows:

Fig. 4 shows the pressure thickness graph for a Diesel oil and a white oil. Both oils yield definite minimum values and give curves of rather different shape, the Diesel oil showing a final film thickness almost twice as large as that of the white oil in spite of its much lower viscosity.

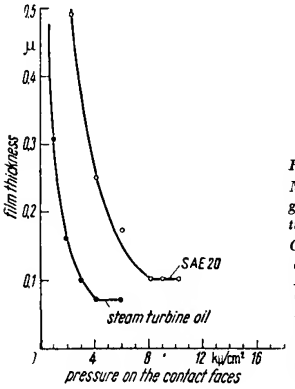

Fig. 5.
Measurement of film thickness of an engine lubricating oil SAE 20 and a steam turbine oil

Characteristic data	*SAE 20*	*Turbine oil*
d_{20}	0.893	0.900
Flp. o. T. °C	181	200
CT %	0.33	0.56
NZ	0.12	0.01
VZ	0.34	0.04
V_{20} °E	19.87	20.00
V_{50} °E	4.19	4.17
VP	2.19	2.19

Fig. 5 shows the curves for two oils of low viscosity, a straight engine lubricating oil of the SAE 20-group and a steam turbine oil, the first one showing a considerably larger film thickness. The results obtained with the four engine lubricating oils are shown in Fig. 6.

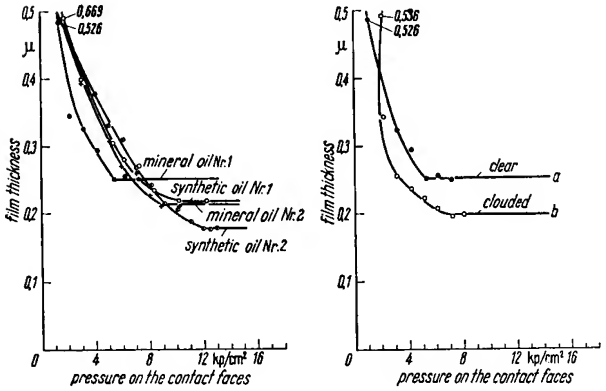

Fig. 6. (on the lef) Measurement of film thickness of engine lubricating oils
Fig. 7. (on the rig it) Change of film thickness of the engine lubricating oil No. 1

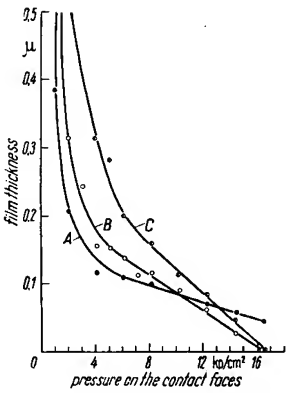

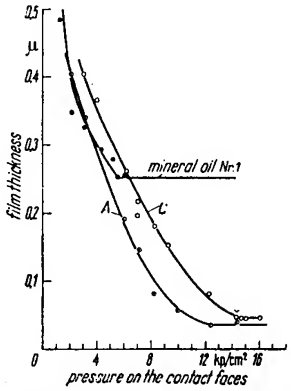

Fig. 8. (on the left) Measurement of film thickness of various phosphoric acid esters
Fig. 9. (on the right) Measurement of film thickness of the mineral oil No. 1 with phosphoric acid esters

Fig. 6 also indicates the high degree of sensitivity of the thickness measurements of films with regard to differences in the oil proper, even if the differences are so small that they cannot be detected by chemical analysis.

Fig. 7 shows the changes in the results of thickness measurements of oil films due to traces of water.

Judging by the results obtained there can be no doubt that the thickness of each of the oil films tends towards a definite characteristic value with increasing pressure, although the structures of the oils vary considerably as is indicated by the Conradson-test which yielded very different values for the various oils submitted to the tests.

However, the differences between the final values are so small that no definite relation between these values and the constitution of the oils could be discerned. We had expected that the mineral oil No. 2 would give the thickest oil film. In the case of the synthetic oils, exhibiting the same Conradson-test results, the final film thicknesses are not nearly alike. The fact that the final film thicknesses can be strongly influenced by other factors is shown in Fig. 7, where small traces of water in the oil induced a thickness difference of 0.052 μ.

Further measurements of film thicknesses were carried out with oils containing certain chemical compounds added for the purpose of increasing the pressure resistance of the lubricating oils. The following three chemical compounds were used: –

A. Thio-phosphoric acid ester of the normal fatty alcohols C_{7-9},

B. Tricresyl phosphate,

C. Phosphoric acid ester of the normal fatty alcohols C_{7-9}.

Fig. 8 shows the results obtained. The curves do not tend towards a definite value, as expected, but approach the H_0-value of the pressure plate. In spite of the fact that the chemical compounds selected for these tests were characterized by strong dipole-moments, strongly adhering layers could not be detected.

The addition A, which still permitted the formation of a definite film thickness at a pressure of 16.4 kp/sq. cm., was present in an amount of 1% by volume. This mixture was used in order to determine the direction in which the film thickness of the basic oil would change (Fig. 8, curve *A*).

The same basic oil was mixed with 3% by volume of the compound C. The final film thickness determined is shown in Fig. 8, curve *C*, while the measuring results for the two oil mixtures are shown in Fig. 9. The measured values of the film

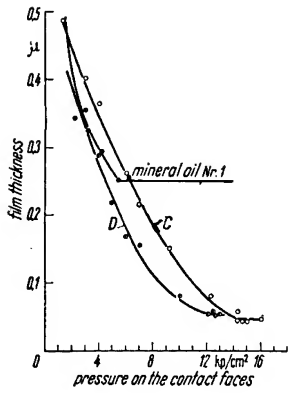

Fig. 10.
Measurement of film thickness of the mineral oil No. 1 (curve D) after measurement of the mixed oil C with the same set of plates

thicknesses of the two oil mixtures lie so closely together that they cannot be used for classification.

On the basis of previous measurements carried out separately for the basic oils and the compounds mentioned, it was to be expected that the final film thickness of the mixtures would become smaller. It was however a surprise to find that these additions exerted such a strong effect. According to the theory that the lubricating properties of oils improve with growing thickness of the film, these high-pressure additions should have induced considerable deteriorations in the lubricating properties of the basic oils, while practical experience has shown that high-pressure additions actually exert a protecting effect on the gliding surfaces of high-duty lubricated bearings.

The results of the thickness measurements of the films thus do not bear any relation to the behaviour of the oils under practical operating conditions. As to our measurements with mixtures, it was found that the surfaces of the measuring plates had changed to such an extent that they had become useless for further measurements, although there changes could not be detected by the usual optical methods.

After measuring the alloyed oils it had been intended to re-use the plates again for the measurement of straight oils. They were therefore cleaned in accordance with the specifications stated above, but the oils subsequently tested in these plates yielded results entirely different from those expected.

Fig. 10 indicates this phenomenon. The set of plates used only for the measuring of straight oils showed for mineral oil No. 1 the characteristic curve with a final film thickness of 0.252 μ. After the addition of chemical compounds according to Fig. 9 we obtained the curve C. After cleaning the plates they were again used for the measurement of basic oils without additions, yielding the curve D. These peculiar phenomena were noticed at all measurements of mixed oils, and the plates could then be used for the testing of straight oils only after regrinding and polishing them.

3. Conclusions

Our measurements were carried out with plates of very little surface roughness, such as cannot be attained under practical operating conditions. The final film thicknesses of the liquids and oils between two even surfaces measured by us did not exceed the value of 0.3 μ. The remaining film will therefore be unable to cover all the unevennesses encountered under normal bearing conditions.

The present opinion that during initial movements of sliding surfaces only the highest points of the uneven surfaces remain in actual contact and that the pressures involved therefore act only on a small part of the entire bearing surface has not been disproved by the results of our experiments. For this reason erosive corrosion must still be considered part of boundary friction; chemical compounds with active constituents (phosphoric acid-thiophosphoric acid), such as the additions selected by us for our measurements, will accelerate this process and thus help to form a more advantageous sliding surface.

In view of the results of our measurements we therefore believe that the final film thickness cannot be employed as a characteristic parameter for the practical valuation of an oil.

TRA 93

Literature

[1] *Ubbelohde:* Die „statische Tragfähigkeit" der Schmieröle und eine „neue Öl-Kennzahl". Kolloidzeitschrift (1952) No. 2/3 pp. 120—140.

By Dr.-Ing. O. Henkler,
Institut für Post- und Fernmeldewesen, Berlin [1])

A New Method to Measure Non-linear Distortions

The well-known harmonic-distortion method is not suited for the measurement of non-linearity in high-grade low-frequency or carrier frequency transmission. The frequently applied differential tone method has the disadvantage of possessing only a limited selectivity and of giving erroneous results due to the occurrence of modulation products with the same frequency, and this becomes particularly significant in carrier frequency transmission. The present paper suggests a new combination factor method to measure non-linear distortions in which the above disadvantages are eliminated.

In communication by low-frequency and carrier transmission, the non-linear distortions impair intelligibility and, in addition, reduce the operating range. Therefore, in telephony the spacing between the signal oscillation frequencies and the noise voltages caused by non-linearities is required to be above 6 Np at the ends of the transmission lines, and even above 10 or 13 Np in case of some long-distance communication equipment. According to the present recommendations of the CCI, the amplitudes of the harmonics appearing at the output of communication equipment are used to characterize and to measure non-linearity. This harmonic-distortion method, however, possesses the disadvantage that the harmonics to be measured are often outside the transmission range

[1]) From a paper read on October 2nd, 1956, at the Conference of Measuring Technique and Automatization in Budapest. Translation of the German Publication in Nachrichtentechnik Vol. 7 (1957) No. 4 pp. 145—147.

(Fig. 1), and that the amplitudes of modulation products within the transmission range, which may produce considerable distortions, escape measurement.

For instance, in a carrier-frequency amplifier for simultaneous amplification of the signal oscillations of 12 telephone subscribers in the frequency range between 12 and 60 kc/s, the square and cubic modulation products from several oscilla-

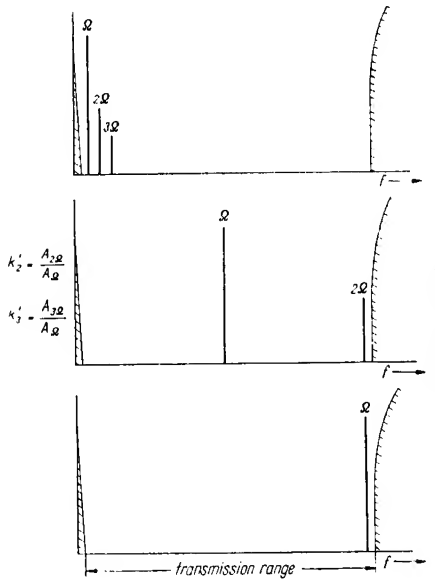

Fig. 1
Modulation products at the output of the object under test when measuring by the harmonic-distortion method

tions of equal amplitude, such as appear at the amplifier output, with the combination frequencies

$$\omega_1 - \omega_2 = 45 - 14 = 31 \text{ kc/s and}$$
$$\omega_1 - \omega_2 + \omega_3 = 45 - 25 + 17 = 37 \text{ kc/s}$$

give distortions which are larger in frequency as well as amplitude than can be determined by measuring the harmonics with the frequencies $2\,\omega_1 = 90$ kc/s and $3\,\omega_1 = 135$ kc/s at the output of an amplifier with a limited frequency band. The two modulation products mentioned, which lie within the transmission range and thus actually distort the signal, have amplitudes that are by 0.7 Np and 1.8 Np, respectively, greater than those of the harmonics as may be seen from the power series expansion of the non-linear relation between amplifier output current and input voltage.

For this reason the differential tone method is often made use of to measure non-linear distortion in carrier-frequency equipment, i. e., the object to be tested is modulated with two oscillations of equal amplitude and constant frequency band Δf (Fig. 2). Here, in order to characterize the non-linearity of the object under test, the modulation products appearing at the output with the frequency $\Omega - \omega$, or $2\,\Omega - \omega$ and $\Omega - 2\,\omega$, are chosen and their amplitudes are compared with those of the two test oscillations. In this method of measuring the differential tone factor, the cubic distortion is not determined directly, but only after an additional transposition into the frequency range $\Omega - \omega$ of the test filter.

In this method, too, the modulation products characterizing the non-linearity do not always lie within the transmission range of the object under test. Furthermore, the differential tone method has the disadvantage that the results may be inaccurate or misleading including modulation products that should not be used for the experimental determination of non-linear distortion, but cannot be excluded if they lie near to the oscillations to be measured and have a larger amplitude (e. g. $A_{\Omega-\omega} > A_{\Omega-2\omega}$), or even the same frequency.

Similar disadvantages may be found in another double-tone method for measuring non-linearities, namely the modulation factor method where the object under test is modulated with two oscillations of different amplitudes.

In order to avoid these difficulties a new method to measure non-linear distortions is suggested in the following.

It is a modified difference tone method where the object to be tested is likewise modulated with two measuring oscillations of equal amplitude, though not with a constant frequency separation but with an optimum separation to be selected for each particular case. The properties of the non-linear system are then characterized by a combination factor, viz., the ratio between the amplitude of a certain modulation product with a selected combination frequency that is present at the output due to non-linearity on one hand and the amplitude of one of the two test oscillations on the other.

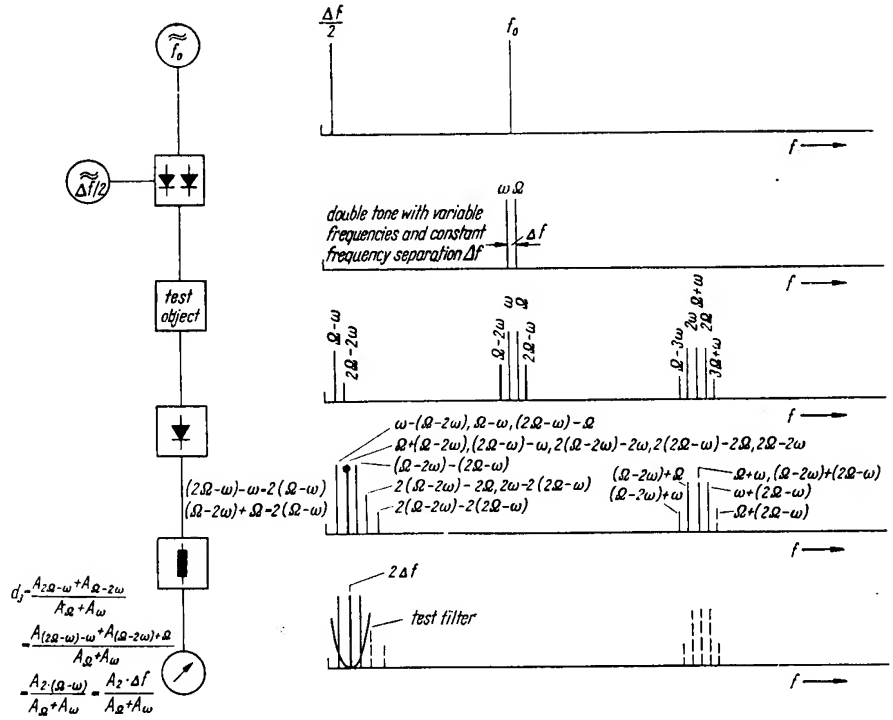

Fig. 2
Measurement of cubic distortion by the differential tone method

This combination factor method is based upon an appropriate choice of the frequencis for the two test oscillations (frequencies Ω and ω) and, in addition, upon an appropriate selection of square and cubic modulation products within the transmission range of the four-pole under test.

Since the expression for the combination frequencies, when referred to the frequency Ω of one of the test oscillations, i. e.,

$$\left(\frac{\pm q\Omega \pm p\,\omega}{\Omega}\right) q, p = -\infty \cdots + \infty$$

depends only on the frequency ratio $\frac{\omega}{\Omega}$ of the test oscillations, it is possible to select for the measurement of non-linearity those values of $\frac{\omega}{\Omega}$ for which the combination frequencies have a constant percentage frequency separation (Fig. 3).

As an example, let us take an object with a transmission range of 12 to 60 kc/s. Only one test filter is required. Its own transmission range can be chosen more or less arbitrarily, but let it be assumed in the present case to be near the upper transmission limit, i. e., near 60 kc/s. According to Fig. 3, the modulation products with the combination frequencies $\Omega + 2\,\omega$, $2\,\Omega - \omega$, and $3\,\Omega$ will then be suited for the measurement of the cubic distortions, and that with a frequency ratio of the two test oscillations as indicated by Fig. 4.

In the given example, the frequency separation between the modulation products to be used for the determination of non-linearity and the undesirable ones lies between 11% and 50%. Hence a good compromise can be obtained between the demand for a large number of test oscillations distributed over the entire transmission range of the object under test and the demand for a selectivity of the test filter that can be economically realized.

It might be mentioned that the ratio of the amplitude of each modulation product selected for this method to the amplitude of the higher harmonic used hitherto as a criterion of non-linearity, can be determined in a simple way from the general power series expansion of the non-linear relation between output current and effective input voltage characterizing the object under test. Therefore, this method makes it possible to measure the frequency-dependent non-linearity of a system with the aid of various

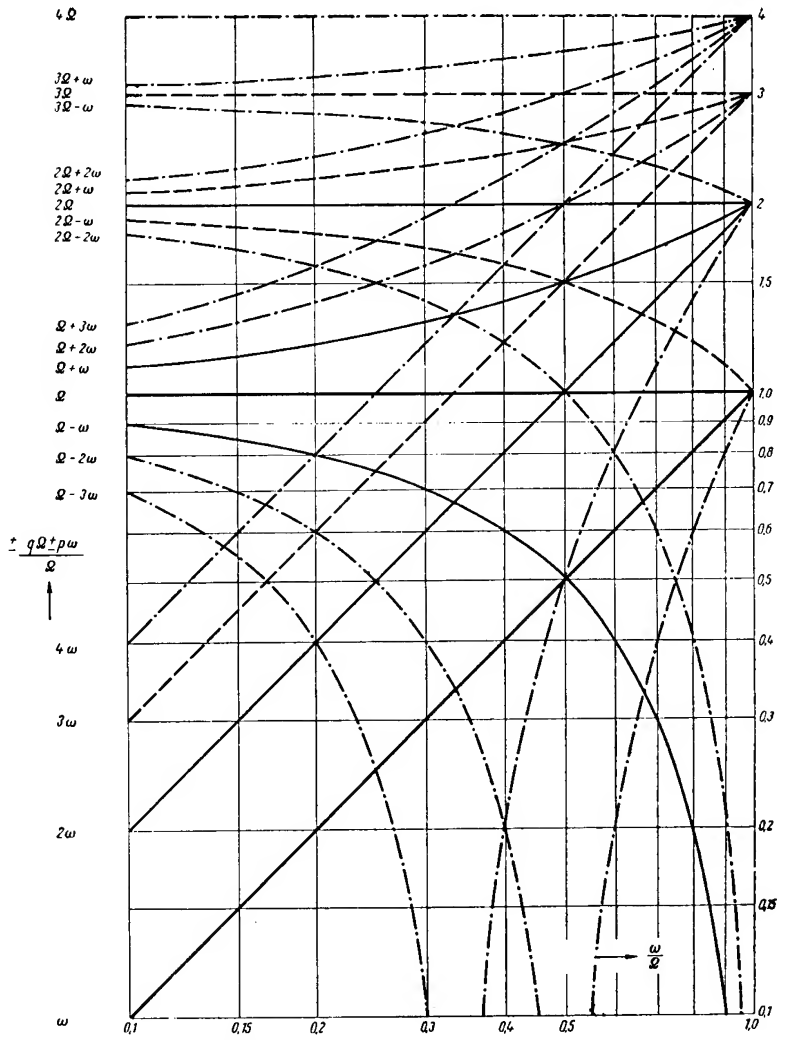

Fig. 3. Modulation products $\frac{\pm q\,\Omega \pm p\,\omega}{\Omega}$ *as function of* $\frac{\omega}{\Omega}$

Fig. 4. Measurement of cubic distortion (Range 12 to 60 kc/s, filter frequency Ω *— 60 kc/s)*

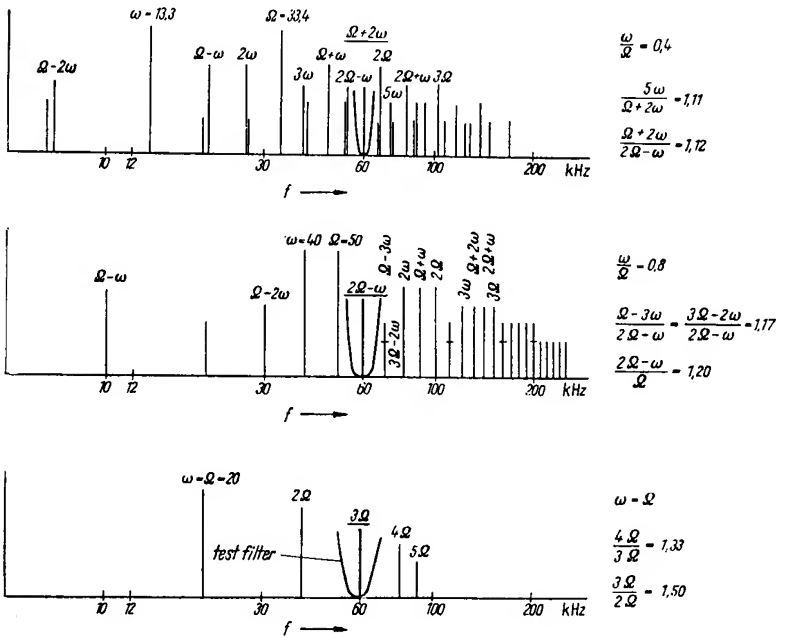

frequencies distributed over the transmission range, which, in addition, may belong to different modulation products (Fig. 4). The combination factor method as described here, possesses a further advantage – referred to the same modulation products (e. g., with the frequency $2\Omega - \omega$) – it is more sensitive than the measurement of cubic distortions by the method shown in Fig. 2 with an amplitude of the interfering oscillation to be measured that is reduced by double modulation. True, the new procedure has the disadvantage that only relatively few points of the transmission range are used, due to the economic restrictions on the quality of the test filter. In practice, however, these points will suffice for carrier-frequency equipment which, in general, possesses a non-linearity that varies continuously with the frequency. Apart from this, it is possible to determine the distorting effect of non-linearities with the aid of noise voltages which correspond better to the spectral distribution of speech than but one or two representative sinusoidal oscillations.

Such measuring methods which use noise voltage generators and noise voltage meters have long since proved useful for the investigation of complete carrier systems because the carrier frequency selection filters provided in these systems may be utilized. Here, too, the novel graphical representation of Fig. 3 can be used to advantage in order to determine the modulation products [2].

Finally, for the testing of carrier-frequency four-poles (such as modulators and amplifiers) not possessing any special selection in their transmission range, measuring procedures have been suggested recently which filter out a "gap" from a noise band and measure the noise voltage component contained in such a gap [1], [4], this gap being shifted over the carrier-frequency transmission range. For the time being, however, no measuring equipment is known which would allow to measure narrow or broad noise bands with a definitely limited amplitude in gaps to be shifted over a carrier transmission range with a sufficient accuracy and with means that would be more economic than those of other well-known methods for the measurement of non-linear distortions. Furthermore, the relation between the permissible power contents of such limited noise bands and the admissible total LF-noise at the end of the carrier voice communication line is not known, nor is the relation between the noise of such limited bands and the noise attenuation which is still generally used for the characterization of non-linearity.

As long as such noise measuring methods have not given any practically applicable results, the described combination factor method should be recommended at least for the carrier-frequency field where it can replace the less adequate methods of harmonic-distortion or differential tones. TRA 98

Literature

[1] *Darré, A.:* Methoden zur Messung nichtlinearer Verzerrungen im Tonfrequenzgebiet. Frequenz Vol. 9 (1955) No. 3/4.
[2] *Henkler, O.:* Ermittlung störender Modulationsprodukte. Radio und Fernsehen (1956) No. 4.
[3] *Henkler, O.:* Über die Nichtlinearität von Trägerfrequenz-Verstärkern. Nachrichtentechnik Vol. 6 (1956) pp. 455 and 456.
[4] *Wolf, M. W.:* Zur Untersuchung nichtlinearer Verzerrungen von Vierpolen durch Signale mit kontinuierlichem Spektrum. J. d. techn. Physik (UdSSR) Vol. 24 (1954) No. 11.

The State of Cable Engineering in the Light of the New VDE-Regulations

By E. Doerfel, Chief Engineer, VEB Kabelwerk Oberspree, Berlin [1])

The publication of the new VDE[2]) Supplementary Regulations (Standards) for power cables, as well as the new Material specification gives occasion to comment on construction and application of the various types of cable.

In the field of power cables there is in the first place a pronounced tendency for economizing on copper and lead, i. e., more aluminium must be used as core and sheathing material and more plastics as high-tension overhead line insulation material for lead-uncovered high-tension cables. The Second Five Year Plan demands that until 1960 the proportion of copper to aluminium used in cable production should be reduced to 33.5 : 66.5 (Fig. 1). Furthermore, cable production should increase to 200% and the production of aluminium to 250%. The total export (which includes a considerable share of cables) should be raised to 170%.

To the great number of cable designs already known still further designs will be added because not all copper- and

[1]) Translation of the German Publication in Deutsche Elektrotechnik Vol. 11 (1957) No. 7 pp. 313—316.
[2]) VDE — Association of German Electrical Engineers.

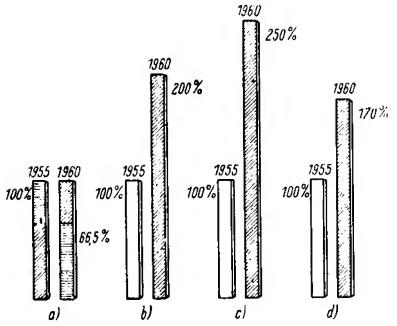

Fig. 1. Objects of the Second Five Year Plan
a) Copper and aluminium consumption
b) Cable production
c) Aluminium production
d) Export

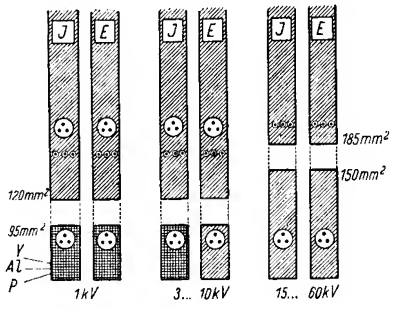

Fig. 2. Survey concerning the permitted use of lead sheathings
I Indoor cables
E Underground cables
Three core cables
Single-core cables

lead-covered cable types can be replaced by copper- and lead-uncovered cables. For particular cases, above all for the export, copper- and lead-covered cables have still to be produced. Tables 1 and 2 and Fig. 2 give a survey in accordance with the Material Specification No. 158, published on 12th November, 1946. In all other cases, the core material is aluminium and the sheathing is aluminium or plastics. The cable types concerned are by no means new, but for some types their range of application has now been extended according to the VDE-regulations 36.0255/2.57, 36.0270/2.57, 36.0271/2.57, and 36.0272/2.57.

Table 1. Copper cores are permitted for:

No.	Cable type	Notes
1	Actuating cables	
2	Control cables	
3	Steering cables	Only up to 0.0093 sq. in. (6 mm²)
4	Measuring cables	
5	Crane cables	
6	Shaft cables	
7	Cables for underground mines	
8	Marine cables	All cross-sections
9	River and deep sea cables	
10	Cables for lubricating oil pumps[1])	
11	Cables laid in rooms with danger of explosion	All cross-sections
12	Cables laid in work rooms of the chemical industries[2])	

[1]) Of turbines, generators, or compressors.
[2]) If there is a danger of corrosion when using aluminium as core material

Table 2. Lead sheathings are permitted for:

No.	Cable type	Tension kV	Cross-section (mm²)	Laying indoors	Laying underground
1	Paper core cables	···1	120···400	+	+
2	Paper core cables	3···10	6··· 95	—	+
3	Paper core cables	3···10	120···400	+	+
4	Paper core cables	15···45	all[1])	+	+
5	Cables for mines	all	all		
6	River cables	all	all		
7	Deep sea cables	all	all		
8	Cables contacting potash salts	all	all		
9	Rubber covered cables	all	all[2])		

[1]) From 185 mm² only as single-core cable.
[2]) The cables may be fitted with lead sheathings, if this is in accordance with the relevant regulations in force for these cables.

Table 3. Symbols and abbreviations for the more important power cables

Cable type Symbol)	Characteristic	Abbreviations (Examples)	
Y	Cables having sprayed-on plastics sheathing	NAYYBA	NAEYYBA
P	Cables having wound plastics sheathing	NIAPB-R	—
Y (PR)	Cables having sprayed-on plastics sheathing and concentric central core	NAYuFY (PR)	NAHEYuFYBA (PR)
P (BR)	Cables having wound plastics sheathing and concentric central core	NAPuFY (PR)	NAHEuFPBA (PR)
Ka	Cables having aluminium sheathing	NAKaBA	NAEKaBA
K	Cables having lead sheathing	NAKBA	NAEKBA

The range of application of cables made of plastics has been increased to 10 kV so that the well-known designs of the metal-uncovered cables must be adapted to the requirements of the higher tensions. In the new VDE-regulations mentioned above the new state of cable engineering is already taken into account.

Table 3 explains the symbols and abbreviations used for the most important high-tension cable types (Y-, P-, Ka-, and K-cables). Their range of application according to cross-section and tension is shown in Table 4. Figs. 3 and 4 show the basic design of the metal-uncovered cables without and with concentric conductor, respectively.

The cables with insulation and sheathing made of sprayed plastics are made with and without armouring. The cables without armouring, however, are only allowed to be used indoors and only for tension as high as 1 kV. In place of the omitted padding and armouring the NYY- and NAYY-cables are constructed with reinforced sheathing made of plastics. These unarmoured plastics cables are of nearly the same design as the plastics lines NYM. Nevertheless, the type NYY is counted as "cable", because it is stronger dimensioned and, consequently, admitted for higher tensions (Fig. 5). The leadless power cables are most frequently used as actuating cables, viz.
NYY-cables with armouring for interiors, or
NKaB-cables with armouring for interiors, and
NKaB-cables without armouring for underground laying.

In case of plastics cables having large core cross-sections it is advisable not to use the belted insulation Y-type, but the YE-type (SL-cable or three-core cable with three lead sheathings, one per core) (Fig. 6), because it consumes less plastics material and has a greater flexibility. The fact that the cable ends need not be fitted with sealed cable ends (Fig. 7) and that differences of level do not matter, is generally considered by the user as a particular advantage of the plastics cable.

Contrary to Y-cables, the P-cables (indoor cables having reinforced plastics winding sheathing must always be with armouring (abbreviation: NIAPB-R).

The PR-cables (underground and indoor cables admitted on trial) having concentric conductors are fitted with a concentric layer of flat or round aluminium wires which may be used either as guard wires or, in case of three and a half- or four-core cables, as centre core. These cables thus comprise only three stranded main cores and one concentric centre core. As a plastics sheathing is provided around the concentric core, any special armouring or coating with asphalt may be omitted (NAYuFY). In the first place, the use of concentric cores is meant to offer a reliable shielding from contact, instead of the unsafety involved with the provision of steel tape armouring which is destroyed by rust in the course of time so that it can no longer fulfil the important protective function.

Current Carrying Capacity of Underground Y-Cables

On this subject some remarks are necessary because very often the relevant instructions contained in VDE 36.0271 are not observed. As stated in Fig. 8, Y-cables carrying d. c. only have a current carrying capacity of 50% of the VDE-table values when laid underground. In case of d. c. and indoor installation the current carrying capacity can be based on the full table values. The reduction of the current carrying capacity need not be considered for control and actuating Y-cables, since then the power transmitted is so small that the heat generated in the cables can be neglected for all practical purposes.

Single-Core Cables with and without Armouring

By using single-core cables the current carrying capacity and consequently the transmission capacity may be raised in

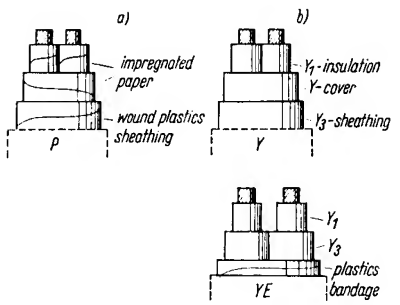

Fig. 3. Metal-uncovered cables for tensions from 1—10 kV without concentric central core
a) for dry and moist rooms
b) for indoor and underground laying

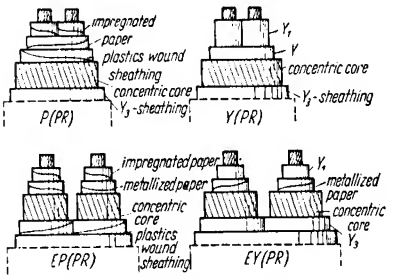

Fig. 4. Metal-uncovered cables for tensions from 1 — 10 kV with concentric central core

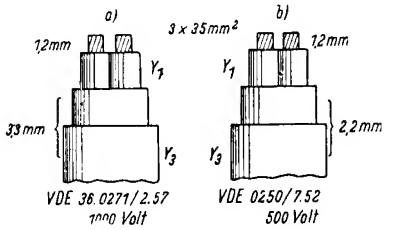

Fig. 5. Technical comparison between plastics cable and plastics wire
a) plastics cable
b) plastics wire

accordance with the informations of the load tables VDE 0255/7.51 without increasing the cross-section or one may use a smaller core cross-section for a given transmission capacity (Figs. 9 and 10). A disadvantage of the single-core cables to be operated by a. c. is that they must not be fitted with steel tape armouring. In such cases where an armouring is absolutely necessary, the single-core cables may be fitted with an open steel wire armouring which offers mechanical protection not only in the axial, but also in the transverse direction.

When using single-core cables, which in themselves are much thinner than three-core cables, small cross-sections should be avoided, because thin cables easily kink and break in case of careless laying. It is not practical to lay more than 820 ft. (250 m) lengths of unarmoured single-core cables within a township, in which case the minimum cross-section should be 0.186 sq. in. (120 mm²). In case of single-core cables having open steel wire armouring the laying lengths generally should not be more than 1312 ft. (400 m) in which case a cross-section of 0.148 sq. in. (95 mm²) should be considered as the lowest limit (Fig. 11). Even when used as neutral wire the single-core cable for a. c. operation must have no closed magnetizable armouring – hence also no steel tape armouring – because the 50-cps-asymmetric current flowing in the conductor would produce eddy currents in the tape armouring. Moreover, an excessively large inductive drop of potential would occur.

Power Cables Interfering with Communication Lines

For a long time it was customary to observe a minimum distance of 12 in. (30 cm) between power and communication cables, no matter whether the lines were parallel or crossing each other (VDE 0101 § 18). In case of single-core cables arranged side by side the communication cables were

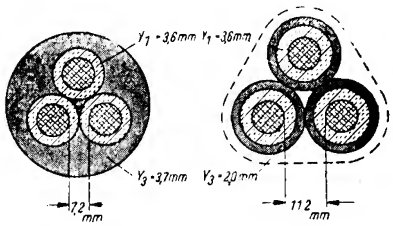

Fig. 6. Plastics consumption of 6 kV-cables
a) Belted insulation NAYYBA
3 × 0.2335 sq. in. (150 mm²) · $Y_1 + Y_3$ = 5.04 lb/yd (2500 kg/cm)
b) Three-core cable NAEYYBA
3 × 0.2325 sq. in. (150 mm²) · $Y_1 + Y_3$ = 3.8302 lb/yd (1900 kg/km)

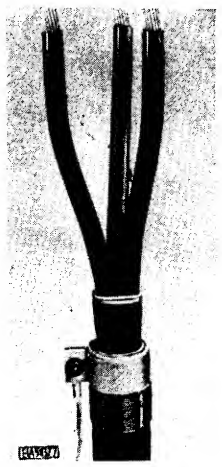

Fig. 7. Plastics cable without sealed cable end

Table 4. Applications of the more important types of power cable

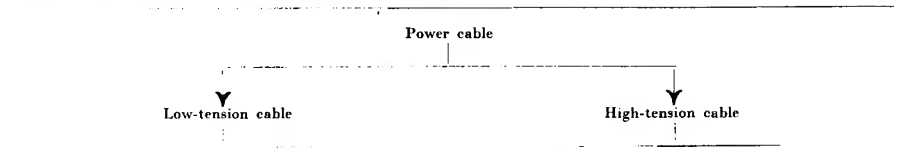

max. 0.148 sq. in. (95 mm²)	from 0.186 sq. in. (120 mm²)	max. 0.148 sq. in. (95 mm²)	from. 0.186 sq. in. (120 mm²)	max. 0.148 sq. in. (95 mm²)	from 0.186 sq. in. (120 mm²)	all cross-sections	all cross-sections
Y-cable P-cable Ka-cable	K-cable	Y-cable — Ka-cable	K-cable	Y-cable P-cable Ka-cable	K-cable	K-cable [1]	K-cable [1]

[1]) From. 0.287 sq. in. (185 mm²) only as single-core cable.

laid zigzag above the three power cables in order that the power current inductions mutually compensate their effects on the communication cables. Interferences have – as far as known – not occurred in the telecommunication system. As far as the interests of telecommunication are concerned, the triangular arrangement of the single-core cables is the most favourable one. The arrangement of the cables side by side requires their regular stranding, similar to overhead lines. This, however, is difficult to realize if three operating

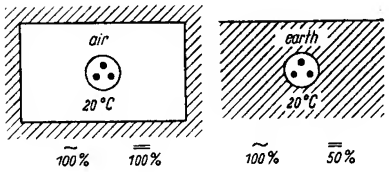

Fig. 8
Current carrying capacity of plastics cables

a) Indoor laying	Kind of current ~	Kind of current ⎓
Current carrying capacity	100%	100%
Overtemperature	35° C	35° C
Core temperature	55° C	55° C
b) Underground laying	**Kind of current ~**	**Kind of current ⎓**
Current carrying capacity	100%	50%
Overtemperature	35° C	9° C
Core temperature	55° C	29° C

belted insulation cable	single core cable	
240mm²	240mm²	240mm²
J = 100%	J ab. 115%	J ab. 125%
240mm²	185mm²	150mm²
J = 100%	J ab. 100%	J ab. 100%

Fig. 9
Current carrying capacity of three-sheath and single-core cables for tension above 10 kV

three-sheathing cable	single core cable x	single core cable x
J = 100%	J ab. 103%	J ab. 120%
NAHEKBA	NAHKA	NAHKA
x without armouring		

Fig. 10
Current carrying capacity of belting insulation and single-core cables for tensions from 3 — 10 kV

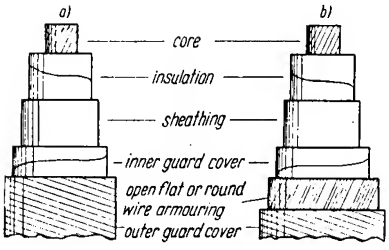

Fig. 11
Minimum cross-sections of single-core cables for laying:
a) within towns, F = 0.186 sq. in. (120 mm²), l = 650 — 820 ft. (200 — 250 m), without armouring;
b) outside of towns, F = 0.148 sq. in. (95 mm²), l = 985 — 1310 ft. (300—400 m), with armouring

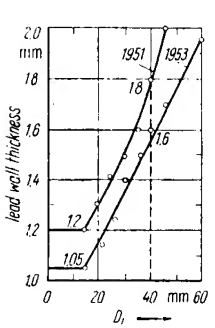

D_i	1951	1952
mm	mm	mm
15	1.2	1.05
20	1.3	1.15
25	1.4	1.25
30	1.5	1.4
35	1.6	1.5
40	1.8	1.6
45	2.0	1.7
50	2.2	1.8
60	2.6	1.95

Fig. 12
Lead wall thicknesses of compound cables

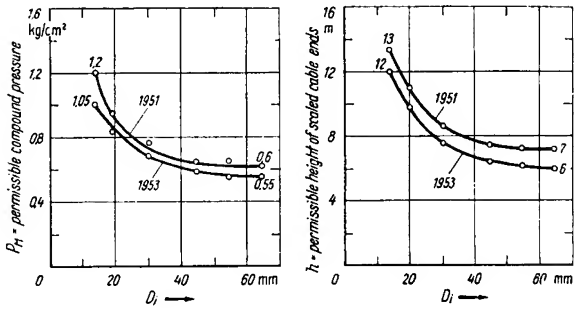

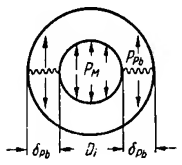

Fig. 13
Permissible pressure or compound cables

$P_M \cdot D_i = P_{Pb} \cdot 2\,\delta_{Pb}$; $P_{Pb} = 106.6$ lb/sq. in (7.5 kg/cm²)

$P_M = 15 \cdot \frac{\delta_{Pb}}{D_i}$; $D_i \approx 21 \cdot \delta_{Pb}$;

$P_M \approx 10.098$ lb/sq. in (0.71 kg/cm²; $\frac{\delta_{Pb}}{D_i} \approx \frac{1}{21}$

cables and one reserve cable are arranged in this manner. The telecommunication cables have become more sensitive to inductive interference and therefore doubts have arisen regarding the inductive effects of polyphase earths. These doubts are even accentuated by the rigid neutral point earthing now planned for high-tension lines, which will make every earth connection a short-circuit. The Technical Branch of Electrical Engineering of the Kammer der Technik, District Great-Berlin, has resolved during its meeting on the 28th February, 1957, to form a technical commitee for preparing, in cooperation with technical experts at home and abroad, new "Directives for Protecting Telecommunication Lines from the Danger of Interference by Three-Phase Power Installations Working at 1 kV or more".

Lead Wall Thicknesses

The lead wall thicknesses corresponding to the GOST-Standards 340–53 have been reduced in 1953 (Fig. 12). The reduction of lead wall thicknesses is a tendency now existing in nearly all countries, because the supply of lead has become a bottle-neck everywhere. This reduction is of mechanical relevance for cable lines with differences in level, first of all for shaft and mast cables. Since lead has a very low creep resistance, the internal pressures produced by the drift of the impregnation compounds towards the lower points of the cable line may cause the danger of lead-sheath expansion and in the end of bursting. As shown in Fig. 13, the maximum permissible level difference is about 23 ft. (7 m) for lead-covered cables using pure lead (VDE 0255/7.51), and only about 20 ft. (6 m) for other lead-covered cables (VDE 36.0255/6.53). This corresponds well to the specifications in GOST 340–53 which e. g. provide for a maximum level difference of 16.4 ft. (5.0 m) for 35 kV lead-covered cables with normal impregnation. In case of alloy-lead sheathings the admissible level difference is about 26 to 33 ft. (8—10 m). In case of greater level differences the lead sheathing must be fitted with a compressive guard bandage, and the insulation should only just comprise the capillary-bound compound, i. e., the surplus should have run off already in the factory after the impregnation process. By way of compensation, the thickness of insulation in high-tension cables is a bit increased. With this basic design, shaft cables of up to 1204 yd. (1100 m) have been manufactured which have proved satisfactory in use. The same points of view are involved with the so-called mast cables, if they are laid higher than about 26 to 33 ft. (8—10 m). In this case the effect of direct solar radiation has also to be taken into account. A metal covering is, therefore, very suitable. It is profitable to use a highly viscous adhesive compound for impregnating

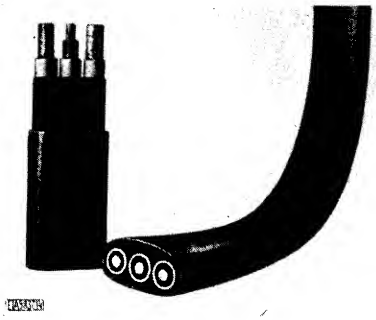

Fig. 14
10 kV three-sheath flat cable
3 × 0.1085 sq. in. (70 mm²) Aldrey. Comparison with a normal shaft cable shows a lead saving of 5.443 lb/yd (2.7 t/km). The total reduction in weight amounts to 14 112 lb/yd (7 t/km)

	3x 120/70	3x 120	3x 120
			
sheathing material	lead	lead	aluminium
cross-section	168 mm²	142 mm²	112 mm²
resistance	0,26 Ω/m central core	1,4 Ω/km sheathing	0,27 Ω/km sheathing

Fig. 15
Use of aluminium sheating as central core

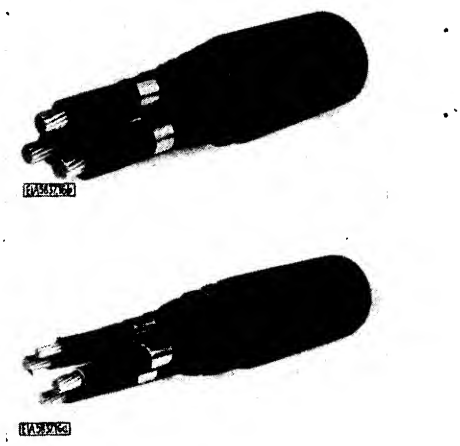

Fig. 16
Samples of aluminium-covered cables
a) four-core aluminium-covered cable
b) three-core aluminium covered cable

the dielectric of such cables in order to prevent or reduce downward-drift. It should be stressed that high viscosity alone is not sufficient and that the compound must also possess good adhesion. In spite of all demands requiring cables for very high masts, careful investigations have shown that in many cases the sealed cable ends can be placed as low as 7—16 ft. (2—5 m) instead of between 33 and 65.6 ft. (10—20 m). When laying at greater heights one has to count with a 20% reduction in the current carrying capacity, and with a further reduction of 15% in case of outdoor temperatures reaching about + 86° F (+ 30° C). When using aluminium-covered cables one may do without the compressive guard bandage, thanks to the considerably higher strength of aluminium compared to lead; however, all the other conditions mentioned above hold good also for aluminium-covered cables.

A VDE-regulation concerning cables with little impregnation is to be issued still this year by the Experts' Committee on Cable and Wires of the Technical Branch of Electrical Engineering of the Kammer der Technik.

The application of mast and shaft cables with dry insulation (sprayed polyvinyl chloride insulation or wound insulation of acetobutyrate foils, and the like, without or with gas pressure) represents a further step of development. A particular design of shaft cables is the flat three-core cable (Fig. 14), which, due to its broad surface, considerably reduces the specific pressure on the guide pulley so that a deformation of the cable cannot occur.

Aluminium Sheathings as Centre Core

Although aluminium sheathings are thinner than lead ones, their resistance is considerably lower than that of lead sheathings, thanks to the relatively good conductivity of aluminium, and for this reason one aspires to employ aluminium sheathings for the central core (Fig. 15). In case of larger cross-sections it is profitable to provide multi-sheath cables with aluminium sheathings instead of belted insulation cables, because the former possess a greater flexibility. In case of three and a half- or four-core cables it is sufficient to use three-sheath cables with the three aluminium sheathings connected in parallel so that the total cross-section amply corresponds to the usual centre core cross-section (Fig. 16). Detailed regulations as o the conditions under which the aluminium sheathings may be used as centre core are now being prepared by the Experts' Committee 2 of the Technical Branch of Electrical Engineering of the Kammer der Technik, and will soon be published.

Summary

The new VDE-regulations 36.0255/2.57, 36.0270/2.57, 36.0271/2.57, and 36.0272/2.57 give information about improvements in cable design and their range of application. The new technical directives of the Material Specification No. 158 concerning raw materials have been interpreted. Furthermore, references have been made to further regulations of the Book of Regulations of German Electrical Engineers (VDE) at present in preparation, concerning cables with little impregnation.

TRA 103

25X1

The Length of the Transition Arc in Road Building

By W. CHRISTFREUND, Dr.-Ing., Weimar [1])

To-day it is generally agreed that the ideal form of the transition curve to be used in road building is the clothoid. This result is based on the condition of uniform change of curvature from $R = \infty$ to $R = R_0$, constant driving speed, and uniform turning of the steering wheel. From these conditions one gets [6], [7]

$$H \cdot L = C = a^2,$$

$$x = \int_0^L \cos \frac{L^2}{2\,a^2} \cdot dL, \qquad y = \int_0^L \sin \frac{L^2}{2\,a^2} \cdot dL$$

and for the clothoid with the parameter 1:

$$x = \int_0^L \cos \frac{l^2}{2}\, dl, \qquad y = \int_0^L \sin \frac{l^2}{2}\, dl$$

After expanding cosine and sine into a series and integrating by terms one obtains:

$$x = 1 - \frac{l^5}{40} + \frac{l^9}{3456} - \frac{l^{13}}{599040} \pm \cdots$$

$$y = \frac{l^3}{6} - \frac{l^7}{336} + \frac{l^{11}}{42240} - \frac{l^{15}}{9676800} \pm \cdots$$

The displacement of the main curve for the inclusion of the transition arc becomes:

$$\Delta h = \frac{l^3}{24} - \frac{l^7}{2088} + \frac{l^{11}}{506880} \pm \cdots$$

In addition to its use as transition curve the clothoid is to be regarded as a tracing element of the same value as the straight line and the circular arc, because, by changing the value of the parameter, one can construct any form of arc [4], [7]. It is not likely, though, that the straight line and the circular arc will be fully replaced by the clothoid, since obviously it is impossible to rebuild all the roads in this way; besides, other factors such as aesthetics, economy, etc., also play a part [9], [10].

There still remains the question of how long the transition arc should be made. As the clothoid is now tabulated for unit parameter and for several other parameter values [6], [7], its use no longer involves any difficulties.

The "Provisional Regulations for Road Building", RAL, 4th Edition 1942 [3] take as basis for the dimension of the transition arcs the following formula which is due to *Örley* [2]:

$$L = \frac{v \cdot g}{\psi} \cdot f$$

where

L = length of the transition arc (m)
v = driving speed (m/s)
g = terrestrial acceleration due to gravity (m/s²)
ψ = jerky acceleration in the time unit (m/s³)
f = coefficient of friction between wheel and roadway.

As the driving speed v in a curve depends on the lateral banking q, the radius H, and the coefficient of friction f, and since the banking has been fixed in RAL to

$$q = \frac{50 \cdot v^2}{g \cdot H}$$

you get, with the further supposition $f = q$,

$$\Delta H = \frac{1}{25600} \cdot \frac{v^6}{H^3} \qquad \text{resp.}$$

$$\Delta H = \frac{1}{1556{,}9} \cdot q^3.$$

The length of the transition arc is then fixed by the formula deduced from the cubic parabola:

$$\Delta H = \frac{L^2}{24 \cdot H}, \text{ or}$$

$$L = \sqrt{24 \cdot H \cdot \Delta H}$$

This deduction, however, involves an inconsistency; for if we suppose that

$$f = q = \frac{50 \cdot v^2}{g \cdot H},$$

the coefficient of friction f enters the basic equation

$$L = \frac{v \cdot g}{\psi} \cdot f$$

as a variable, though it is a constant for each roadway in its given condition. This means that in computing the length of the transition arc the coefficient of friction takes the values

0.02 for $q = 2\%$ 0.04 for $q = 4\%$
0.03 for $q = 3\%$ 0.08 for $q = 8\%$ etc.

while in reality the following values hold for a wet roadway [1], [8]:

mastic asphalt	$f = 0.33$	granite metalling	$f = 0.25$
concrete	$f = 0.33$	basalt metalling	$f = 0.22$
tar	$f = 0.31$		

The computation of the really necessary length of transition arcs is to be based on the assumptions that

1. the driving speed is kept constant throughout the transition arc,
2. the jerk does not surpass a certain limit,
3. the coefficient of friction has a constant value.

According to Fig. 1 this gives the following condition of equilibrium [5]

$$z \cdot \cos \alpha - g \cdot \sin \alpha - (g \cdot \cos \alpha + z \cdot \sin \alpha) \cdot f = 0, \qquad (1)$$

where $z = \frac{v^2}{H}$ means the lateral acceleration.

Of this, the roadway takes up

$$(g \cdot \cos \alpha + z \cdot \sin \alpha) \cdot f,$$

so it remains the free lateral acceleration:

$$c = z \cdot \cos \alpha - g \cdot \sin \alpha.$$

Now the jerk ψ (m/s³) is the rate of change of the lateral acceleration:

$$\psi = \frac{dc}{dt} = \frac{d}{dt}(z \cdot \cos \alpha - g \cdot \sin \alpha).$$

It should be constant in the transition arc. With

$$\cos \alpha = \frac{1}{\sqrt{1 + \tan^2 \alpha}} \quad \text{and} \quad \sin \alpha = \frac{\tan \alpha}{\sqrt{1 + \tan^2 \alpha}}$$

this gives $\psi = \frac{d}{dt}\left(\frac{v^2}{H\sqrt{1 + \tan^2 \alpha}} - \frac{g \cdot \tan \alpha}{\sqrt{1 + \tan^2 \alpha}}\right)$

or, since $\tan \alpha = q$, you have

$$\psi = \frac{d}{dt}\left(\frac{v^2}{H\sqrt{1 + q^2}} - \frac{g \cdot q}{\sqrt{1 + q^2}}\right).$$

[1]) Translation of the German Publication in Straßentechnik, Vol. 5 (1957) No. 7 pp. 82, and 83. Supplement to Bauplanung—Bautechnik Vol. 11 (1957) No. 7.

As the slope should obey the law of curvature, q_d (cross-section like a one-sided lean-to) grows in proportion to the curvature to $q_{ü}$ (raised degree of bank in the curve), and even at the beginning of the transition arc there is a one-sided slant. According to Fig. 2 we have the relation

$$\frac{H_0}{H} = \frac{q - q_d}{q_{ü} - q_d} \quad \text{or} \quad q = \frac{H_0}{H}(q_{ü} - q_d) + q_d.$$

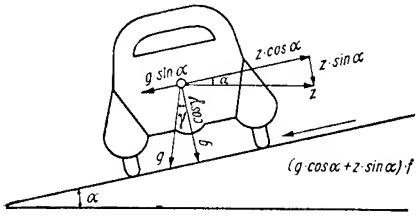

Fig. 1. Diagram of forces when driving through a curve

Hence one obtains

$$\psi = \frac{d}{dt}\left[\frac{v^2}{H\sqrt{1+\left[\frac{H_0}{H}(q_{ü}-q_d)+q_d\right]^2}} - \frac{g\left[\frac{H_0}{H}(q_{ü}-q_d)+q_d\right]^2}{\sqrt{1+\left[\frac{H_0}{H}(q_{ü}-q_d)+q_d\right]^2}}\right].$$

or, since $dt = \frac{dl}{v}$, it is

$$\psi = \frac{dc}{dt} = \frac{d\cdot v}{dl}\left[\frac{v^2}{H\sqrt{1+\left[\frac{H_0}{H}(q_{ü}-q_d)+q_d\right]^2}} - \frac{g\left[\frac{H_0}{H}(q_{ü}-q_d)+q_d\right]^2}{\sqrt{1+\left[\frac{H_0}{H}(q_{ü}-q_d)+q_d\right]^2}}\right].$$

According to equation (1) it is

$$\frac{v^2}{H_0}(\cos\alpha - f\cdot\sin\alpha) - g(\sin\alpha + f\cdot\cos\alpha) = 0,$$

and from this

$$H_0 = \frac{v^2(\cos\alpha - f\cdot\sin\alpha)}{g(\sin\alpha + f\cdot\cos\alpha)} \quad \text{or as } \tan\alpha = q_{ü}$$

$$H_0 = \frac{v^2}{g}\left(\frac{1 - f\cdot q_{ü}}{f + q_{ü}}\right).$$

From this y ou get

$$\psi = \frac{dc}{dt} = \frac{d}{dl}\cdot v\left[\frac{v^2}{H\sqrt{1+\left[\frac{v^2(1-f\cdot q_{ü})}{H\cdot g(f+q_{ü})}(q_{ü}-q_d)+q_d\right]^2}} - \frac{g\left[\frac{v^2(1-f\cdot q_{ü})}{H\cdot g(f+q_{ü})}(q_{ü}-q_d)+q_d\right]}{\sqrt{1+\left[\frac{v^2(1+f\cdot q_{ü})}{H\cdot g(f+q_{ü})}(q_{ü}-q_d)+q_d\right]^2}}\right]$$

and

$$\psi\int_0^L dl = d(v)\left|H\frac{v^2}{\sqrt{}} - \cdots\right|$$

within the limits $H = \infty$ to $H_0 = \frac{v^2(l - f\cdot q_{ü})}{g(f + q_{ü})}$

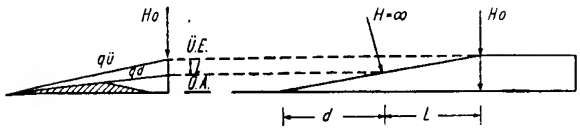

Fig. 2

After integration one obtains

$$\psi\cdot L = v\cdot g\left(f\frac{\sqrt{1+q_{ü}^2}}{1 - f\cdot q_{ü}} + \frac{q_d}{\sqrt{1+q_d^2}}\right).$$

Thus, the length of the transition arc is determined by:

$$L = \frac{v\cdot g}{\psi}\left(f\frac{\sqrt{1+q_{ü}^2}}{1 - f\cdot q_{ü}} + \frac{q_d}{\sqrt{1+q_d^2}}\right).$$

If you put $q_{ü}$ and $q_d = 0$, you get the Örley equation

$$L = \frac{v\cdot g}{\psi}\cdot f.$$

On first sight, it seems to be odd that for decreasing f the length of the transition arc should decrease; rather one would expect that the length of the transition arc should increase for a roadway that is more slippery. One can see, however, that the formula is correct from the fact that for the limit $f = 0$ there is no possibility to build a transition arc.

As a lower limit one may take $f = 0.25$. The jerk ψ still admissible for driving motor vehicles can be taken as 0.5 m/s³. while $g = 9.81$ m/s².

With these values one obtains

$$L = 4{,}905\cdot v\left(\frac{\sqrt{1+q_{ü}^2}}{1 - 0{,}25\,q_{ü}} + \frac{4\,q_d}{\sqrt{1+q_d^2}}\right)$$

The limiting values are given by

1. $q_{ü} = 8\%$ and $q_d = 2\%$
2. $q_{ü} = 2\%$ and $q_d = 2\%$.

With these values you get for L

1. $L = 5.415\cdot v$ (m)
2. $L = 5.229\cdot v$ (m)

or with $v = \frac{V}{3.6}$ (km/h)

1. $L = 1.503$ V (m)
2. $L = 1.45$ V (m).

Thus, $L = 1.5$ V may be used as minimum length of the transition arc.

But we want to stress the fact that this is a minimum. For aesthetic reasons one should always try to make the length of the transition arc larger than 1.5 V.

Literature

[1] *Weil:* Über die Reibungswerte zwischen Rad und Fahrbahn. Dissertation Technische Hochschule Stuttgart (1934).

[2] *Örley:* Übergangsbogen bei Straßenkrümmungen. Verlag Volk und Reich (1937).

[3] *Örley:* Vorläufige Richtlinien für den Ausbau von Landstraßen. Verlag Volk und Reich, 4th Edition (1942).

[4] *Lorenz:* Die Klothoide als Trassierungselemente. Verkehr und Technik (1948) No. 9.

[5] *Krebs:* Der Übergangsbogen im Straßenbau. Berechnung der Klothoide aus der Fahrdynamik. Die Bautechnik (1950) p. 176; (1951) p. 207.

[6] *Vesely, V.:* Klotoida. Technicko – Vedecke Vydavatelstvi, Praha (1952).

[7] *Kaspar, Schürba, Lorenz:* Die Klothoide als Trassierungselement. Ferd. Dümmler Verlag, Bonn (1954).

[8] *Boldizar, V.:* Utepitestan. Tankönyvkiado, Budapest (1954).

[9] *Hering, R.:* Ist die Gerade als Trassierungselement nötig? Straße und Autobahn (1955) No. 2.

[10] *Albrecht:* Ist die Gerade als Trassierungselement zum Aussterben verurteilt? Straße und Autobahn (1955) No. 6.

TRA 101

The Tool-Carrier RS 09

Many years experience in tractor construction has proved a great help to VEB Traktorenwerk Schönebeck in the development of their new types and implements. In particular, the new tool-carrier RS 09 seems to be well suited to solve a major part of the problems involved in the mechanization of agriculture.

The construction principle of the RS 09 is that of a combination of tractor and tools. That means that the design of this tool-carrier is different from that of standard tractors. The tool-carrier can also be used as a light tractor, but will be employed principally for soil cultivation (Fig. 1), harvesting work, and for the preparation of the soil. Inasmuch as many different operations are required for this type of work, the tool-carrier must combine a high capacity with a great variety of possible applications. Thanks to a number of technical innovations and improvements, this purpose was fully attained with the RS 09.

The main components of the RS 09 are the driving axle, the longitudinal girder, and the front axle. The operating power is transmitted to the additional implements from the driving axle, composed of engine- and gear-unit. The longitudinal girder is designed for the attachment and for the transport of these implements. The execution of driving manoeuvres is left to the front axle. The condition for one-man operation is given by the single-holm construction. An unobstructed view and a favourable angle of survey over the additional implements was obtained by other constructive improvements, granting an unencumbered operation. The frame of the RS 09 is composed of a square-section girder and a front axle console. The telescope type front axle is suspended without springs in the front axle console in a swinging way. The ground clearance could be reduced from 480 mm to 240 mm by dividing the axle shanks of the front axle, so that the vehicle, thanks to its low centre of gravity, can be used also under the most difficult conditions and on hilly grounds. Due to its air-cooled Diesel engine the machine operates with a very high efficiency. The engine is not located any more in front of the gear-box, but is flanged-on behind the gear-box. This fact alone grants four special advantages:

1. an increased tractional power due to a favourable location of the centre of gravity;
2. an unobstructed view from the driver's seat;
3. easy accessibility of clutch and gear;
4. the construction of a self-contained driving axle.

The general use of this driving axle was made possible by combining engine and gear into one unit. This construction permits the development and application of new implements suited to the requirements of widely different agricultural operations. The intaken air is led through a cyclon with oil bath filter so that the life expectance of the engine is not impaired even if the air contains a high percentage of dust. A combined exhaust air filter and cyclon installation has been planned as a further improvement, so that in future a nearly dustfree operation will be obtained.

Console and front axle of the RS 09 are adjustable in the driving direction. That means that the wheel distance can be reduced from 2210 mm to 1760 mm. This will facilitate the mounting of additional implements in front of the front axle. Besides the possibilities of adjusting ground clearance and wheel base, also the track gauge of the vehicle can be adjusted within the range of 1250—1670 mm. It can thus be adjusted to the different widths between rows. This fact is of special importance when the tool-carrier is used for cultivation purposes. The telescope pipe of the steering column and the steering mechanism are built into the longitudinal girder and the steering mechanism is fixed to the front axle console. In this way the mounting of implements is made easier and a higher safety against damage is obtained.

The divided steering rods between console and front axle, as well as the telescope pipe axle, can be adjusted according to the track gauge of the vehicle. The main part of the rear axle is formed by the gear, which disposes of $2 \times 4 = 8$ foreward and reverse speeds. Driving speeds between 0.9 and 15 km/h can be obtained in two switching stages. A creeping speed of 0.59 km/h can be obtained in the first speed by throttling the engine. In this way the speeds required for different operations can be maintained.

Seat, steering column, and all control elements are mounted on the gear-box. The changing levers are mounted on the steering column and clearly marked. Axle cones and the double countershaft are fastened to the driving wheel to the right and to the left of the gear-box. The mechanical inner jaw brake is located at the axle cone, in front of the countershaft. There is a flange at the rear side of the gear, to which the engine is attached. This is equipped with a driving clutch. The connecting surface to the tenonshaft gear is formed by the lower side of the gear. The rear tenonshaft is extended by a counter-tenonshaft. Both front and rear tenonshafts can be operated either by the engine or by the wheels. Both shafts work independently of each other, so that there are 8 different possibilities of gear-shifting. This means that any combination of additional implements with suspension in front of, or between the axles, or behind the driving axle, can be used.

A further characteristic of the RS 09 is its great manoeuvreability. An almost pinpoint turning radius can be obtained because of the individual wheel braking and the high turning angle of the front wheels. Driver's seat, steering wheel, and control elements can be reversed, so that it is possible to carry out special operations in a direction opposite to the normal driving direction, without the hazards usually connected with driving backwards. The RS 09 can thus be considered a two-way tractor. New ways of application may be derived from this property, and it should be possible to develop new implements specially adapted to certain tasks.

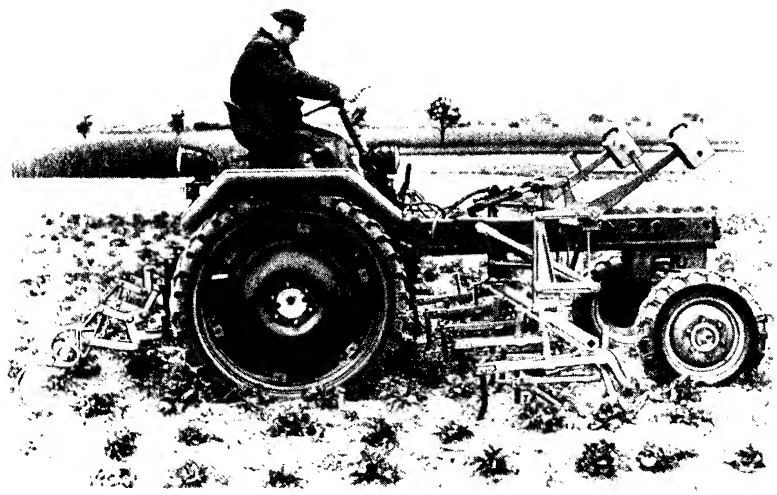

Fig. 1. Tool-carrier RS 09 (manufactured by VEB Traktorenwerk Schönebeck) with attached hoeing machine

Fig. 2. Tool-carrier RS 09 with attached sprayer S 293 with twin nozzle

Fig. 3. Tool-carrier RS 09 with attached sprayer and broad base distributor

The additional implements provided for this tool-carrier are operated by a hydraulic device built into the gear. The output of this device is high enough to operate several tools at the same time, while sparing the physical strength of the operator. The pressure caused on the soil by the tool-carrier is almost the lowest possible, due to its light-weight construction. This will help to avoid damage to the cultures.

In the following a summary is given of the technical data of the RS 09:

Engine: 18 H. P. two-cylinder four-stroke air-cooled Diesel engine (Warchalowski licence construction).

Gear: Eight forward and nine reverse speeds

Driving speed in km/h at 3000 r. p. m. of the engine:

1st speed	0.89	5th speed	4.00
2nd speed	1.33	6th speed	5.95
3rd speed	2.14	7th speed	9.23
4th speed	3.32	8th speed	14.86

Driving speed in km/h at 2000 r. p. m. of the engine:

1st speed	0.59	5th speed	2.66
2nd speed	0.89	6th speed	3.96
3rd speed	1.43	7th speed	6.15
4th speed	2.25	8th speed	9.90

Tenonshaft:

Front and rear according to DIN 9611 (29 × 34.9 × 8.7):

a) driven by the engine
n = 540 r. p. m.

b) driven by the wheels 3.3 km/h at n = 540 r. p. m.

Maximum output of the tenonshaft 15 H. P. at 540 r. p. m. = 20 mkg.

Tyres:

Front: 6.00 - 16 AS Front
Rear: 7.00 - 36 AS

Track gauge: Adjustable to 1250, 1375, 1500, and 1670 mm

Wheel base: Standard 2210 mm, continuously adjustable to 1760 mm

Radius of turning circle: 2.5 - 3.0 m

Weight:	with standard equipment kg	with special equipment kg
Total weight	980	1090
a) front axle load	220	240
b) rear axle load	760	850
Permissible total weight		
a) permissible service load on front axle		1160
b) permissible service load on rear axle		250
c) permissible total service load		1410

Seat: Reversible for foreward and backward driving

Steering: Steering system with a knuckle lever turn of 90°

Brakes: a) mechanical inner jaw driving brake, acting on the differential
b) hand brake, acting also on the brake drum. Special rods for manual operation

Ground clearance: Maximum 480 mm, adjustable to 240 mm

Trailing rail: Field type rail without springs

Hydraulic:
Cogwheel pump with built-on steering cylinder and working cylinders on either side.
Maximum capacity 28 l m, adjustable from 10—28 l/m
Pressure 80 atm. (maximum 100 atm.)
Number of revolution n = 1875 r. p. m.

A number of additional implements are being manufactured by our industry. Among them are for instance: reaping beams, change plows, fertilizer distributors, drilling machines, ejector wheel cultivators, hoeing machines, multiple purpose devices, corn planting machines, squirting and spraying machines (Figs. 2 and 3). Also implements like harrows, rollers, weeders, diggers, and flat reaper binders, as well as all other implements which require a low pulling power can be used as trailers. This makes the RS 09 very economical in all branches of agriculture, whether in field, fruit and vegetable cultivation, in courtyards and meadows, or in forestry. The RS 09 can be used at any time and everywhere in agriculture, independent of season and weather.

Finally it should be mentioned here that further machines based on the principle of the tool-carrier have been designed and put in production; they are variations of the tool-carrier RS 09. In particular, the corn cultivating tractor RS 26, the courtyard tractor RS 27, and the dumper TA 25 will go a long way to close the gaps still existing at the present time in the range of application of the tool-carrier principle.

We shall treat these machines in detail in further articles.

TRA 108 *Steffen*

Instrumentenkunde der Vermessungstechnik

(Theory of Surveying Instruments)

By F. Deumlich and M. Seyfert

This work meets the demand for a reference-book about up-to-date construction of geodetic instruments – a demand all the more justified as great progress has been made during the last 20 years. As will be seen by the title, the book has been confined to the instruments of lower geodesy. Therefore astronomic instruments, theodolites for high-class triangulations, instruments for hydrostatic leveling, and electro-optical range-finders have not been dealt with though the latter are also used for lower geodesy. Likewise instruments for indoor service (cartographic and drawing instruments, planimeters) have been omitted on purpose. The instruments for lower geodesy to be used outdoors are thoroughly and clearly discussed, the examples being chosen mainly from instruments of German and Swiss construction. The book has the following Sections:

1. Fundamentals
2. Instruments for setting out and measuring horizontal angles
3. Instruments for measuring heights and differences in height
4. Devices and instruments for range-finding
5. Instruments for tachymetry.

The first section deals with the fundamentals of optical theory and optical devices. Here level testing and corrections are discussed only in general terms, the detailed investigation being given in the following sections in connection with the instruments concerned.

The second part begins with diopter, mirror, and prism instruments for setting out right or straight angles, followed by a discussion of simple instruments for measuring and setting out horizontal angles of any size, such as scale disk and compass. After pointing to the surveying or meridian gyroscope a detailed description of the theodolite (Fig. 1) and its use is given with due attention to the particularities of the different constructions.

After a short introduction to simple instruments for leveling (water level, ruler, a. o.) the leveling instruments of different construction with extras and their application are described in the third section. Further, the theodolite for measuring vertical angles, the sextant, and the barometers are discussed.

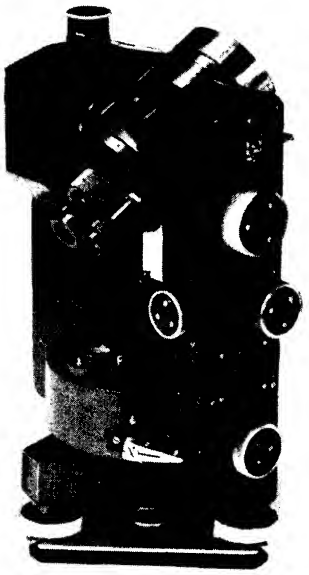

Fig. 1
The theodolite Theo 010 of VEB Carl Zeiss, Jena

The fourth part deals with the instruments for direct range-finding such as stadia rods and surveyor's tapes and their testing. The Jäderin instrument for base measuring is mentioned. The devices and instruments for indirect distance measuring form the main content. Principle, construction, use, and attainable precision of both types, i. e. with target base and with base at the station, are described.

The last part deals with the approved instruments for tachymetry. It is subdivided according to instruments with Reichenbach distance threads, self-reducing or self-computing tachymeters, surveyor's boards, and alidades.

The work is well composed as to subject-matter and illustrated by excellent pictures. It will help the expert to select the most suitable device and to handle it correctly. To the student it is warmly recommended as text-book.

TRB 119 *Koitzsch*

[1]) VEB Verlag Technik, Berlin 1957. DIN B 5. 379 pp., 384 illustr. Full-Leatherine 28.– DM.

HARITH

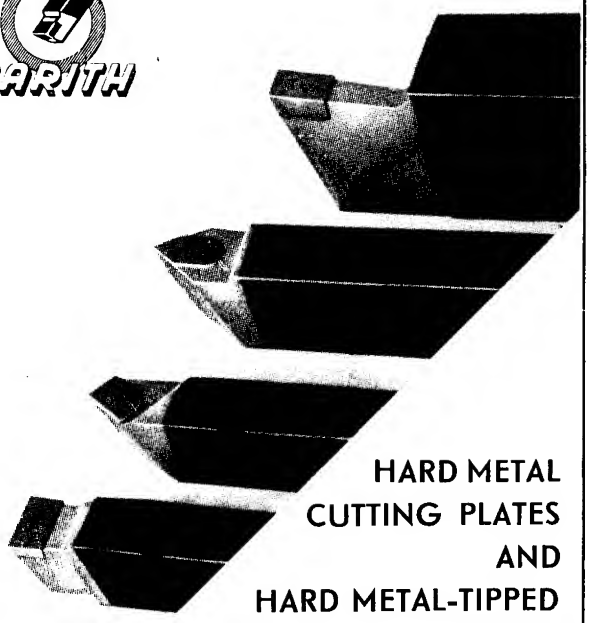

HARD METAL
CUTTING PLATES
AND
HARD METAL-TIPPED
TOOLS

VEB HARTMETALLWERK IMMELBORN
IMMELBORN (THÜR.)

Wegilit

Driving belts
Conveyor belts
— endless and by metre —

Conveyor belts
of all special designes.

The great success:
"Wegilit-Kaschiert"
the layer belt on PVC-basis.

Manufacturer:
H. WERNER GIERMANN
GOTHA/THURINGIA
GERMAN DEMOCRATIC REPUBLIC

VEB (K)
Glasspritzenfabrik Gräfenroda

Medi

Manufacture of
All-Glass Syringes and
Record Syringe Cylinders

Exhibiters of the Leipzig Fair

M+G

Scouring and Polishing Machines
with switch clock —
to be turned by hand or automatically.

Bell form if wanted
with or without rubber lining

VEB MASCHINENFABRIK GREIZ

Wir fertigen:

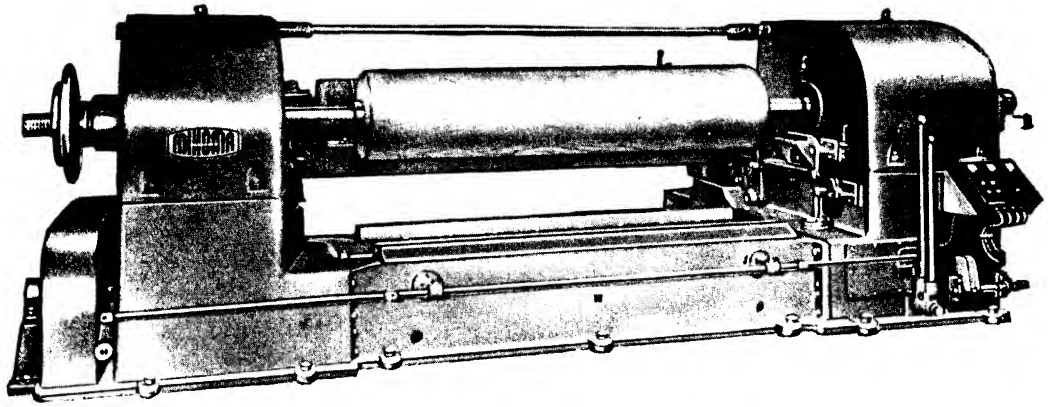

WE MANUFACTURE:

Parallel pendulum saws	PSS
Double edging, ripping and lath cutting saws	DLKM
Circular veneer peeling machines	FRS 8—12
Circular veneer peeling machines	FRS 10—26
Hydraulic hot plate presses, 2 openings	FSP 2
Hydraulic hot plate presses, 4 openings	FSP 4
Hydraulic hot plate presses, 6 openings	FSP 6
Hydraulic hot plate presses, 7 openings	FSP 7
Hydraulic hot plate presses, 8 openings	FSP 8
Hydraulic hot plate presses special construction	
Veneer strip assembly machines	FVM
Automatic knot hole patching machines	AFA
Automatic lath assembling machines	LZM
Planing and moulding machines	HK 20
Finishing planers	PH
Finishing planers	SPH 4
Heavy finishing planers	SPH 8
Wood wool machines	HW
Double end tenoners	DZS
Dovetailing machines	ZSM
Dovetailing apparatus	ZFA
Knot hole drilling machines	ABM
Two drum sanding machines	ZWS 9 and 11
Triple drum sanding machines	DWS 12
Triple drum sanding machines	DWS 18
Scraping machines	ZK 18
Scraper grinding machines	ZKS 18
Rotary cutting machines	RMM

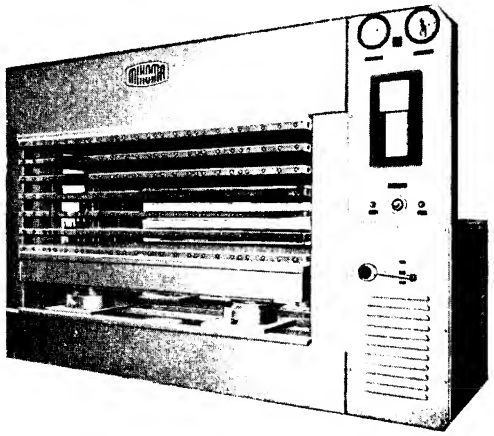

MIHOMA LEIPZIG

HOLZBEARBEITUNGSMASCHINENBAU · LEIPZIG O 5, TORGAUER STR. 43 · PHONE 64321